Annu. Rev. Mar. Sci. 2023. 15:249–75

First published as a Review in Advance on September 15, 2022

The *Annual Review of Marine Science* is online at marine.annualreviews.org

https://doi.org/10.1146/annurev-marine-040422-084555

Annual Review of Marine Science

Modes and Mechanisms of Pacific Decadal-Scale Variability

E. Di Lorenzo,[1] T. Xu,[2] Y. Zhao,[3] M. Newman,[2,4] A. Capotondi,[2,4] S. Stevenson,[5] D.J. Amaya,[2] B.T. Anderson,[6] R. Ding,[7] J.C. Furtado,[8] Y. Joh,[9] G. Liguori,[10,11] J. Lou,[2,4] A.J. Miller,[12] G. Navarra,[13] N. Schneider,[14] D.J. Vimont,[15] S. Wu,[16] and H. Zhang[17]

[1]Department of Earth, Environmental, and Planetary Sciences, Brown University, Providence, Rhode Island, USA; email: e.dilorenzo@brown.edu

[2]Physical Sciences Laboratory, National Oceanic and Atmospheric Administration, Boulder, Colorado, USA

[3]Deep-Sea Multidisciplinary Research Center, Pilot National Laboratory for Marine Science and Technology (Qingdao), Qingdao, China

[4]Cooperative Institute for Research in Environmental Sciences (CIRES), University of Colorado Boulder, Boulder, Colorado, USA

[5]Bren School of Environmental Science and Management, University of California, Santa Barbara, California, USA

[6]Department of Earth and Environment, Boston University, Boston, Massachusetts, USA

[7]State Key Laboratory of Earth Surface Processes and Resource Ecology, Beijing Normal University, Beijing, China

[8]School of Meteorology, University of Oklahoma, Norman, Oklahoma, USA

[9]Atmospheric and Oceanic Sciences Program, Princeton University, Princeton, New Jersey, USA

[10]Department of Physics and Astronomy, University of Bologna, Bologna, Italy

[11]School of Earth, Atmosphere, and Environment, Monash University, Melbourne, Victoria, Australia

[12]Scripps Institution of Oceanography, University of California, San Diego, La Jolla, California, USA

[13]Program in Ocean Science and Engineering, Georgia Institute of Technology, Atlanta, Georgia, USA

[14]International Pacific Research Center and Department of Oceanography, University of Hawai'i at Mānoa, Honolulu, Hawaii, USA

[15]Department of Atmospheric and Oceanic Sciences, University of Wisconsin–Madison, Madison, Wisconsin, USA

[16]Laboratory for Climate and Ocean-Atmosphere Studies, Department of Atmospheric and Oceanic Sciences, School of Physics, Peking University, Beijing, China

[17]Department of Earth and Atmospheric Sciences, University of Houston, Houston, Texas, USA

Keywords

Pacific decadal variability, Pacific Ocean, climate variability, climate change, ocean–atmosphere teleconnections, El Niño–Southern Oscillation

Abstract

The modes of Pacific decadal-scale variability (PDV), traditionally defined as statistical patterns of variance, reflect to first order the ocean's integration (i.e., reddening) of atmospheric forcing that arises from both a shift and a change in strength of the climatological (time-mean) atmospheric circulation. While these patterns concisely describe PDV, they do not distinguish among the key dynamical processes driving the evolution of PDV anomalies, including atmospheric and ocean teleconnections and coupled feedbacks with similar spatial structures that operate on different timescales. In this review, we synthesize past analysis using an empirical dynamical model constructed from monthly ocean surface anomalies drawn from several reanalysis products, showing that the PDV modes of variance result from two fundamental low-frequency dynamical eigenmodes: the North Pacific–central Pacific (NP-CP) and Kuroshio–Oyashio Extension (KOE) modes. Both eigenmodes highlight how two-way tropical–extratropical teleconnection dynamics are the primary mechanisms energizing and synchronizing the basin-scale footprint of PDV. While the NP-CP mode captures interannual- to decadal-scale variability, the KOE mode is linked to the basin-scale expression of PDV on decadal to multidecadal timescales, including contributions from the South Pacific.

1. INTRODUCTION

Traditionally, the low-frequency variability of the climate system has been described in terms of modes of decadal variability, sometimes called oscillations due to their spatial (seesaw-like) structure, such as the Pacific Decadal Oscillation (PDO) (Mantua et al. 1997), the North Pacific Gyre Oscillation (NPGO) (Di Lorenzo et al. 2008), the South Pacific Decadal Oscillation (SPDO) (Hsu & Chen 2011), and the Interdecadal Pacific Oscillation (IPO) (Power et al. 1999). However, most of the named modes do not exhibit a preferred timescale of variability (specifically, they are not periodic), since they are designed to capture statistical patterns that efficiently represent strong low-frequency variance on interannual to multidecadal timescales, rather than low-frequency dynamical modes of the Pacific climate system (Monahan et al. 2009). Nevertheless, modulations of these patterns are linked to significant impacts on weather and extremes of the Americas and Asia (Alexander 2010, Deser et al. 2010, Dai 2013, Wei et al. 2021, Xu et al. 2021) and to large-amplitude transitions in marine ecosystems (Mantua et al. 1997, Hare et al. 1999, Bograd et al. 2019, Yati et al. 2020, van der Sleen et al. 2022). Recent examples of these modes impacting extremes include marine heatwaves and droughts over North America in 2013–2015 and 2019 (Swain 2015, Amaya et al. 2016, Di Lorenzo & Mantua 2016, Seager & Henderson 2016, Capotondi et al. 2019, Holbrook et al. 2019, Xu et al. 2021) and tropical storms (Chu & Clark 1999).

Building on a previous review focused on the predictability of the Pacific climate modes (Liu & Di Lorenzo 2018), this article focuses on discussing significant advances in our understanding of the fundamental mechanisms, including global- and basin-scale teleconnection dynamics, that act to energize the temporal and spatial structures of the dynamical modes of Pacific decadal-scale variability (PDV). To this end, this review is organized as follows. We begin by reviewing the dominant statistical modes of observed ocean and atmosphere variability of the Pacific basin

(Section 2) and provide a first-order understanding of how these patterns are forced in the extratropics and how they are related to the tropics. We then outline an empirical dynamical modeling approach (Section 3) that helps identify the dynamical modes of the Pacific system and provides insight into the mechanisms that energize the low-frequency climate variance. These mechanisms are then analyzed in detail (Section 4) to review our current hypotheses of the role of basin-scale teleconnections and tropical–extratropical coupling dynamics. Given that most of our understanding is constrained by one realization of the observed world, we discuss (Section 3) how robust and stable the mechanisms of PDV are when considering an ensemble view of climate where the same world can lead to different realizations of the patterns and mechanisms of Pacific climate. We close with a summary of the main mechanisms and future challenges (Section 5).

2. STATISTICAL PATTERNS OF PACIFIC DECADAL-SCALE VARIABILITY

The global decadal-scale variability of sea surface temperature anomalies (SSTa) shows that the tropical and North Pacific, together with the North Atlantic, are the most energetic regions of low-frequency (e.g., 8-year low pass) variability. Previous analyses of global SSTa have documented that several modes of PDV are main contributors to both global climate variability (Messie & Chavez 2011) and fluctuations of the global warming trend, such as the 1998–2013 hiatus (Meehl et al. 2011, Kosaka & Xie 2013, Watanabe et al. 2013, England et al. 2014). These results are evident by decomposing the variance of the global 8-year low-pass SSTa into its first two empirical orthogonal functions (EOFs). The first decadal global mode (**Figure 1*a***), explaining 34% of the total decadal variance, shows loading in the Pacific basin that resembles the classical El Niño–like pattern of decadal variability (Zhang et al. 1997). The second global mode (**Figure 1*b***) is characterized by strong loading in both the northeast Pacific and the central tropical Pacific, where tropical Pacific decadal-scale variability (TPDV) is typically a maximum (Power et al. 2021). Together, these two global modes capture the different flavors of PDV. This can be visualized and quantified by defining a PDV mode that is equal to the sum of global mode 1 and global mode 2 (i.e., a rotation in the plane of the first two EOFs). The resulting pattern (**Figure 1*c***) is now dominated entirely by the Pacific basin, and the temporal evolution of the PDV mode is strongly and significantly correlated with the IPO ($R = 0.96$) (**Figure 1*e***) and all other indices of the major named modes of Pacific climate variability. In fact, we can reconstruct each of the Pacific climate modes' indices as a simple linear combination of the two global mode time series as $a \cdot$ global mode $1 + b \cdot$ global mode 2 (**Figure 1*e***), where the coefficients a and b represent the relative weighting of the two modes.

We also show the pattern arising from taking the difference between the two global modes (**Figure 1*d***), which recovers an interhemispheric mode of opposite signs whose corresponding time series is strongly correlated with that of the Atlantic Multidecadal Oscillation ($R = 0.9$) (Knight et al. 2006, Deser et al. 2010, Levine et al. 2017) and its Pacific footprint (Y.-M. Yang et al. 2020). Regardless of how we combine these global modes, it is clear that PDV plays a major role in global low-frequency climate variability. We also note that similar results are obtained from a Pacific-only analysis—that is, one based on recomputing the two leading EOFs from the 8-year low-pass SSTa only within the Pacific basin between 62°S and 62°N (**Figure 1*a*,*b***). This similarity indicates that this variance decomposition is robust in the Pacific sector and suggests that PDV is linked to the dynamics of other basins, as is evident from the spatial expressions of the PDV global modes in the North Atlantic (e.g., the Atlantic Multidecadal Oscillation pattern) (Kucharski et al. 2016, Screen & Francis 2016, Levine et al. 2017, Deepa et al. 2019, Nigam et al. 2020, X.-Y. Yang et al. 2020).

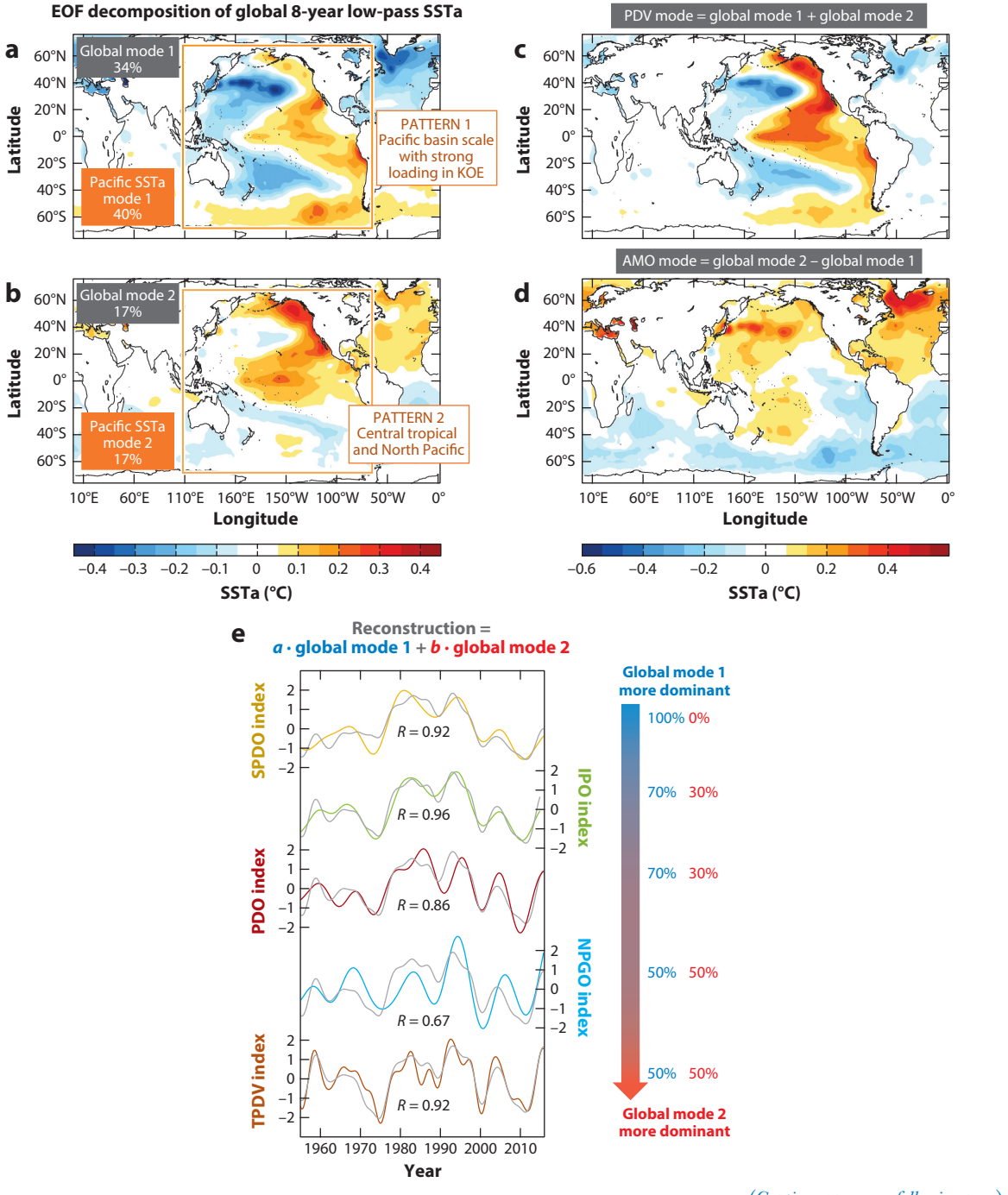

(*Caption appears on following page*)

Figure 1 (*Figure appears on preceding page*)

Decomposition of the global-scale low-frequency SSTa variance. The standard deviation of 8-year low-pass NOAA ERSST v3b (1950–2019) is decomposed into the first two EOFs, referred to as global mode 1 (panel *a*) and global mode 2 (panel *b*). By adding and subtracting the first two global EOFs, we recover the canonical pattern of the PDV mode, which is equal to global mode 1 + global mode 2 (panel *c*), and that of the AMO mode, which is equal to global mode 2 − global mode 1 (panel *d*). Together, the first two global EOFs capture most of the spatial structures and temporal variability of the known modes of Pacific climate variability, such as the IPO, PDO, SPDO, NPGO, and TPDV. This is quantified by reconstructing the time series of each of the Pacific modes with a linear combination of the two global modes (panel *e*). In panels *a* and *b*, the orange square indicates the Pacific basin between 62°S and 62°N. Abbreviations: AMO, Atlantic Multidecadal Oscillation; EOF, empirical orthogonal function; IPO, Interdecadal Pacific Oscillation; KOE, Kuroshio–Oyashio Extension; NOAA ERSST v3b, National Oceanic and Atmospheric Administration Extended Reconstructed Sea Surface Temperature version 3b; NPGO, North Pacific Gyre Oscillation; PDO, Pacific Decadal Oscillation; PDV, Pacific decadal-scale variability; SPDO, South Pacific Decadal Oscillation; SSTa, sea surface temperature anomalies; TPDV, tropical Pacific decadal-scale variability.

2.1. Patterns of Extratropical Decadal-Scale Variance

To provide a first-order understanding of the origin of the dominant patterns of PDV in the extratropics, we also need to consider the mean circulation of the atmosphere and its variability. Over the Pacific basin, the time-mean sea level pressure (**Figure 2*a***) is characterized by the presence of large-scale pressure systems, such as the winter Aleutian Low (AL) and summer North Pacific High in the Northern Hemisphere and the South Pacific High in the Southern Hemisphere. These pressure systems undergo modulations in their positions and strength on all timescales, whose variability can be quantified by the EOF modes. Specifically in the North Pacific, the leading EOF mode of sea level pressure anomalies captures a change in the position and strength of the AL (Trenberth & Hurrell 1994, Chhak et al. 2009) (**Figure 2*b***), while the second mode tracks changes in the strength of the mean North Pacific circulation, with a dipolar structure (**Figure 2*c***) colocated over the centers of action of the North Pacific High and AL. This second leading atmospheric mode has been named the North Pacific Oscillation (NPO) (Rogers 1981, Linkin & Nigam 2008). Similarly, in the South Pacific, the leading mode of variability in atmospheric sea level pressure anomalies, excluding the Antarctic region south of 50°S, captures changes in the mean circulation of the South Pacific High (**Figure 2*d***) and is referred to as the South Pacific Oscillation (SPO) (You & Furtado 2017).

The atmospheric modes described above (**Figure 2**) have an oceanic footprint in SSTa and other physical–biological variables, since they drive an ocean response through changes in surface winds and heat fluxes that project onto the dominant modes of extratropical ocean decadal variability. Specifically, in the North Pacific, the AL mode drives the largest fraction of variance in the SSTa pattern of the PDO (first EOF of SSTa) (Mantua et al. 1997, Zhang et al. 1997) (**Figure 2*e***). Similarly, the NPO drives the NPGO, which is defined as the second EOF of sea surface height in the northeast Pacific (Di Lorenzo et al. 2008) and closely tracks the second EOF of SSTa—also referred to as the Victoria mode (Bond et al. 2003) (**Figure 2*f***). Additionally, the boreal winter (January–March) expression of the NPGO tracks the SSTa footprint of the North Pacific Meridional Mode (NPMM) (Chiang & Vimont 2004, Amaya 2019). In the South Pacific, the SPO drives the dominant mode of SSTa, the SPDO (Chen & Wallace 2015, Lou et al. 2019) (**Figure 2*g***). However, in contrast to the North Pacific, the SPO undergoes substantial seasonal fluctuations, and during boreal spring (February–April), the oceanic footprint of this atmospheric mode consists of a different SSTa pattern that emerges as the second mode of SSTa variability and is referred to as the South Pacific quadrupole pattern (Zheng & Wang 2017, Lou et al. 2021) or the South Pacific Meridional Mode (SPMM) (Zhang et al. 2014, Larson et al. 2018, Zhao & Di Lorenzo 2020) (**Figure 2*h***).

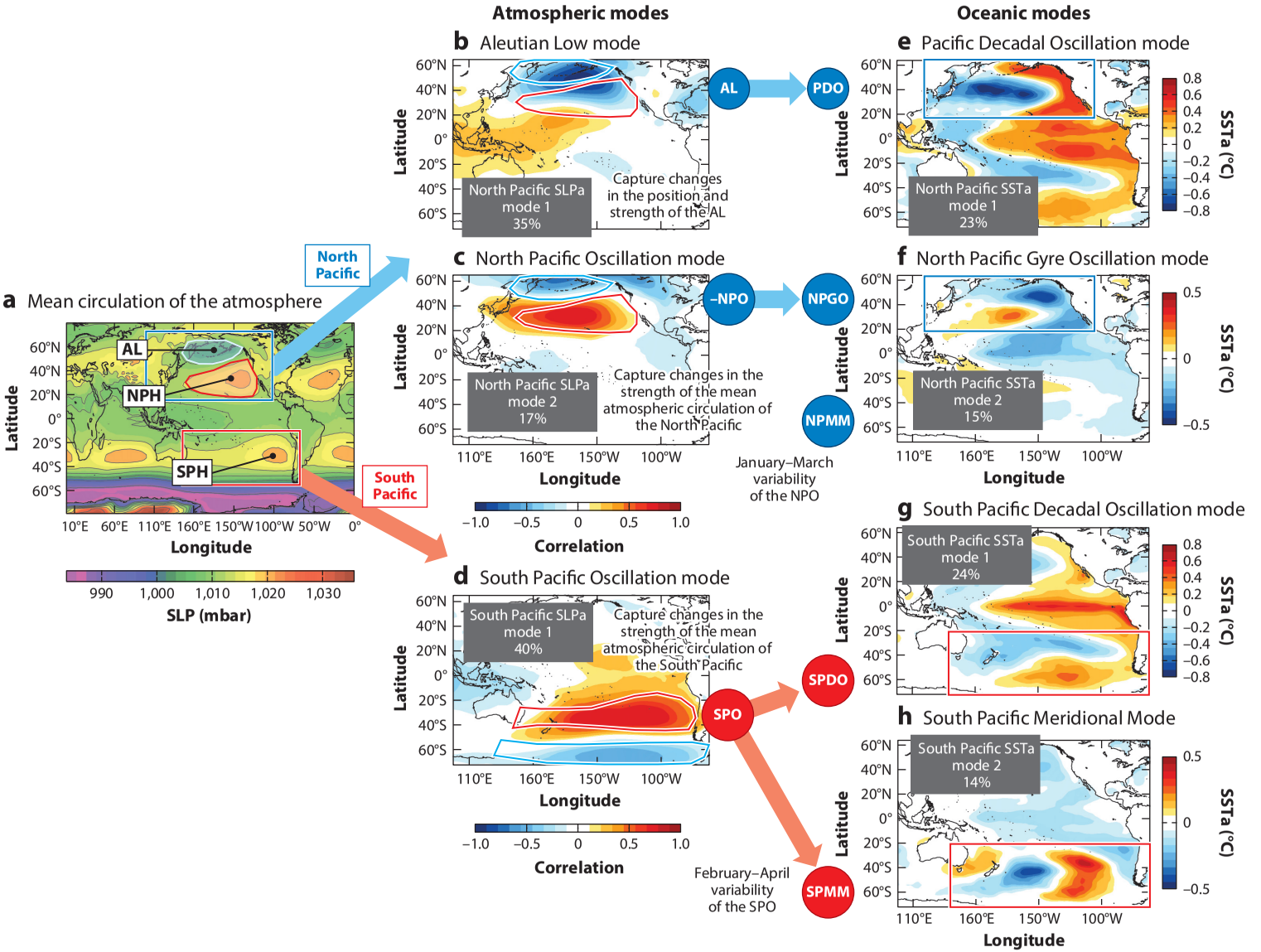

(Caption appears on following page)

Figure 2 (*Figure appears on preceding page*)

The statistical patterns of PDV. Panel *a* shows the mean atmospheric SLP. Panels *b* and *c* show the first two dominant EOFs of SLPa in the North Pacific, tracking the AL and NPO modes, respectively, and panels *e* and *f* show their respective oceanic expressions, the PDO and NPGO/NPMM. Similarly, panel *d* shows the dominant modes of South Pacific SLPa, tracking the SPO; panel *g* shows its oceanic expression, the SPDO; and panel *h* shows its seasonal expression, the SPMM. The red and blue outlined shapes in the atmospheric modes (panels *b–d*) mark the locations of the mean SLP highs and lows, respectively. The rectangles in the mean circulation (panel *a*) and oceanic modes (panels *e–h*) represent the areas where the SSTa EOFs are defined. Abbreviations: AL, Aleutian Low; EOF, empirical orthogonal function; NPGO, North Pacific Gyre Oscillation; NPH, North Pacific High; NPMM, North Pacific Meridional Mode; NPO, North Pacific Oscillation; PDO, Pacific Decadal Oscillation; PDV, Pacific decadal-scale variability; SLP, sea level pressure; SLPa, sea level pressure anomalies; SPDO, South Pacific Decadal Oscillation; SPH, South Pacific High; SPMM, South Pacific Meridional Mode; SPO, South Pacific Oscillation; SSTa, sea surface temperature anomalies.

Atmospheric variability is largely on daily through seasonal timescales, so it may be approximated with a white power spectrum on the decadal timescales of interest here. The ocean, however, integrates and thereby reddens this atmospheric forcing (Newman et al. 2003, Rudnick & Davis 2003, Schneider & Cornuelle 2005, Vimont 2005, Deser et al. 2010)—that is, the ability of the ocean to integrate over time the high-frequency variability of the atmosphere and essentially act as a low-pass filter. This process helps drive low-frequency (i.e., red power spectrum) variability in the oceanic PDV modes. The timescale over which the ocean can accumulate the atmospheric forcing is set by the internal memory of oceanic dynamics, including the ability of the mixed layer to store heat, oceanic wave adjustments to wind perturbations, and other longer-timescale memory dynamics, such as reemergence (Deser et al. 2003, Namias & Born 1974) and the subduction of heat anomalies in the ocean subsurface (Schneider et al. 1999; Taguchi & Schneider 2014; Pozo Buil & Di Lorenzo 2015, 2017).

A fundamental model used to explain oceanic reddening was first introduced by Hasselmann (1976) in a one-dimensional equation:

$$\frac{\mathrm{d}O(t)}{\mathrm{d}t} = \alpha \cdot A(t) - \frac{O(t)}{\tau}, \qquad 1.$$

where the rate of change of the anomalies of an oceanic variable $O(t)$ on the left-hand side is driven by atmospheric anomalies $A(t)$ scaled by a conversion factor α, and where the oceanic anomaly exponentially decays with a timescale of τ, representing the memory of the oceanic variable being considered. When discretized into a difference equation, this model is equivalent to an autoregressive model of order 1 (AR-1), which is a known low-frequency filter. Using this simple model, one can reconstruct the time series of the PDO, NPGO, and SPDO by simply forcing Equation 1 with the atmospheric time series of the AL, NPO, and SPO modes, respectively, and using $\tau = 8$–12 months, which is the typical decay rate of SSTa in the extratropics (Chhak et al. 2009, Di Lorenzo et al. 2013). By correlating the output of Equation 1 with basin-scale SSTa, we recover the global footprints of the PDV modes (e.g., **Figure 2*e–h***).

Although the simple one-dimensional model in Equation 1 works very well in recovering the oceanic modes and providing a simple explanation of the emergence of these patterns, it is important to recognize that it does not allow us to separate and understand the large-scale dynamics that energize the variance of the atmospheric modes, including feedbacks from the extratropical and tropical oceans captured in the oceanic modes themselves. Consequently, several studies have aimed to identify different drivers of the PDO, NPGO, and SPDO by separating the atmospheric variable on the right-hand side of Equation 1 into its extratropical and tropical teleconnection components (Schneider & Cornuelle 2005, Shakun & Shaman 2009, Lou et al. 2019, Zhao et al. 2021b). In fact, as we discuss in more depth in Section 4, teleconnection dynamics to and from the tropics play a major role in shaping the low-frequency variability of the Pacific basin and its extratropical decadal modes.

2.2. ENSO-Like Tropical Decadal Variability Pattern

Most of the dominant modes of Pacific SSTa (e.g., the PDO and SPDO; **Figure 2*e*,*g***) show a clear signal in the tropics, highlighting their links to the El Niño–Southern Oscillation (ENSO) and TPDV (Power et al. 2021). ENSO is the dominant phenomenon of tropical Pacific variability on seasonal to interannual timescales, and its teleconnections to the extratropics impact ocean–atmosphere and ecosystem variability across the entire Pacific basin (Bjerknes 1968, Alexander et al. 2002). Moreover, ENSO can both influence and be influenced by extratropical variability (Chang et al. 2007, Larson & Kirtman 2014, Zhang et al. 2014, Zhao & Di Lorenzo 2020, Capotondi & Ricciardulli 2021, Lou et al. 2021). In fact, the effects of these teleconnections (further described in Section 4.1) are also reddened by extratropical oceanic memory into ENSO-like decadal variability (Di Lorenzo et al. 2015), which is captured in the PDV pattern (**Figure 1*c***). This ENSO-like SSTa pattern emerges in the low-frequency expression of the PDO, NPGO, SPDO, and IPO and is consistent with the TPDV (Zhao & Di Lorenzo 2020), defined as the leading EOF of the 8-year low-pass SSTa over the tropical Pacific between 5°S and 5°N. Consistent with this finding, the time series of the TPDV mode is highly correlated with the 8-year low-pass indices of all the major statistical modes of Pacific climate (**Figure 1*e***).

These simple analyses indicate that the statistical modes of low-frequency Pacific variability capture different flavors of basin-wide and local-scale decadal variability (e.g., Zhang et al. 2018). Practically, while the modes and patterns of variance defined from EOFs provide important hints of the key mechanisms of PDV, these modes do not track individual processes but are the result of several dynamical mechanisms that rely on tropical or extratropical teleconnections with ENSO and ocean–atmosphere coupling.

3. DYNAMICAL MODES OF PACIFIC DECADAL-SCALE VARIABILITY

While the statistical modes of PDV provide a useful description of Pacific low-frequency climate variability and are routinely used to identify and predict how climate variability impacts biogeochemical cycles, marine ecosystems, weather, and climate extremes (Mantua et al. 1997, Hare & Mantua 2000, Yati et al. 2020), the objective of this review is to identify and understand the physical mechanisms of the dynamical modes of Pacific climate variability. The computation of climate modes through EOFs imposes an orthogonality constraint in the spatial patterns and temporal evolution of the modes. However, as noted above, in the low-frequency regime, these modes converge to similar patterns of variability (e.g., ENSO-like) and are spatially nonorthogonal outside the geographical regions where the modes are defined (see, e.g., the PDO and SPDO in **Figure 2*e*,*g***). This finding indicates that the orthogonality constraint is an artifact of the definition and not a physical constraint. Moreover, eigenmodes of physical dynamical systems are typically not orthogonal (e.g., Monahan et al. 2009), due to asymmetries both in space (such as differing regions of strong or weak gradients) and between variables (such as when one variable appears in the tendency equation of a second variable but not vice versa). In fact, strong evidence exists that the modes obtained with statistical approaches, such as ENSO and the PDO, result from the constructive superposition of several nonorthogonal dynamical modes (Farrell 1988, Penland & Sardeshmukh 1995). Unfortunately, computing the dynamical modes of the Pacific climate system is nontrivial and relies on our ability to perform an eigenmode analysis of the true dynamical operator controlling the evolution of this system. While a full knowledge of such an operator is hard to obtain apart from very simplified physical models, it is possible to use empirical approaches to approximate this operator from observations, in an inverse sense, and determine its eigenmodes. Here, we use one such empirical dynamical model of Pacific SSTa to examine the spatial and temporal variability of observed dynamical modes.

3.1. An Empirical Dynamical Model for Pacific Climate

In Section 1, we introduced a simple one-dimensional AR-1 model (Equation 1) to illustrate how the ocean can integrate the atmospheric forcing and filter the low-frequency variability of the atmosphere. We can more generally extend this model to a multivariate formulation to approximate the evolution of a suitably averaged climate anomaly state vector $\mathbf{x}(t)$ as

$$\frac{d\mathbf{x}}{dt} = \mathbf{L}\mathbf{x} + \boldsymbol{\xi} \qquad 2.$$

(Hasselmann 1976, Penland & Sardeshmukh 1995), where $\mathbf{L}$ is a linear dynamical operator and $\boldsymbol{\xi}$ is a vector of temporally white noise. Although linear, this model can accommodate the nonlinear portion of climate dynamics through the noise term under the assumption that the temporal evolutions decorrelate much faster than the linear dynamics. For example, nonlinear forcing of the ocean by weather occurs on timescales that are typically much shorter than oceanic memory timescales and may therefore by approximated by a linear feedback term plus a white noise remainder (Frankignoul & Hasselmann 1977), an approximation that may also be extended to include advection by strong oceanic currents (Frankignoul & Reynolds 1983).

From Equation 2, the most likely solution of the state of $\mathbf{x}$ at $t + \tau$ is given by the ensemble average evolution,

$$\hat{\mathbf{x}}(t+\tau) = \mathbf{G}(\tau)\mathbf{x}(t) = \exp(\mathbf{L}\tau)\mathbf{x}(t), \qquad 3.$$

with the noise terms providing the ensemble spread about this mean (i.e., less likely outcomes). Equations 2 and 3 are commonly referred to as a linear inverse model (LIM) (Penland & Matrosova 1994, Penland & Sardeshmukh 1995), which has been widely used to predict and simulate Pacific climate variability (e.g., Newman et al. 2011, Capotondi & Sardeshmukh 2017, Lou et al. 2020, Xu et al. 2021, Capotondi et al. 2022). In Equation 3, the propagator $\mathbf{G}(\tau)$ can be determined empirically from the observed instantaneous and lag covariances as $\mathbf{G}(\tau) = \mathbf{C}_\tau\mathbf{C}_0^{-1}$ and has a direct relationship to the dynamical operator $\mathbf{L} = \text{logm}(\mathbf{G})/\tau$. Thus, the eigenvectors of $\mathbf{L}$ capture lagged feedbacks among the different components of the state vector, both locally and teleconnected, and not simply patterns maximizing the lag 0 covariances, as in traditional EOFs and principal component analysis. The eigenmodes of $\mathbf{L}$ constitute an empirical approximation of the dynamical modes of the system,

$$\mathbf{L}\mathbf{U} = \mathbf{U}\boldsymbol{\Lambda}, \qquad 4.$$

where $\mathbf{U}$ is the matrix of eigenvectors [whose spatial patterns ($\mathbf{u}_i$) are the ith column of $\mathbf{U}$] and $\boldsymbol{\Lambda}$ is the diagonal matrix of eigenvalues (λ_i). Then the modes may be sorted by their decay time, $|1/\text{Re}(\lambda_i)|$.

The corresponding time series of each mode requires additional determination of $\mathbf{V}$, the eigenvectors of $\mathbf{L}$'s adjoint. These are determined by $\mathbf{V}^{\text{H}} = \mathbf{U}^{-1}$, such that $\mathbf{L}^{\text{H}}\mathbf{V} = \mathbf{V}\boldsymbol{\Lambda}^*$, where a superscript H denotes the conjugate transpose and an asterisk denotes the conjugate. The time series is then $\alpha_i(t) = \mathbf{v}_i^{\text{H}}\mathbf{x}(t)$, where $\mathbf{v}_i$ is the ith column of $\mathbf{V}$. That is, the time series of each eigenmode is obtained by projecting the data on that eigenmode's adjoint, rather than by projecting the data on the eigenmode itself, as is done when determining the time series corresponding to an EOF. Note also that, while the eigenmodes are not orthogonal, they remain independent of each other; that is, the climate state anomaly $\mathbf{x}(t)$ can be reconstructed from the sum of the individual modal contributions, $\alpha_i(t)\mathbf{u}_i$. However, due to the modal nonorthogonality, the variance of $\mathbf{x}(t)$ cannot be reconstructed as the sum of the variances of the eigenmodes, again in contrast to EOFs.

For this review, we computed the eigenmodes of $\mathbf{L}$ using a state vector $\mathbf{x}(t)$ constructed from SSTa over the Pacific region (60°E–70°W, 70°S–62°N) from three reanalysis data sets: Hadley

Centre Sea Ice and Sea Surface Temperature (HadISST) (1900–2017) (Rayner et al. 2003), National Oceanic and Atmospheric Administration Extended Reconstructed Sea Surface Temperature version 3b (NOAA ERSST v3b) (1950–2019) (Smith et al. 2008), and Ocean Reanalysis System 4 (ORAS4) (1958–2016) (Balmaseda et al. 2013). Given that the computation of these eigenmodes is done through an empirical approach, the use of different data sets allows us to identify which modes are robust and how sensitive they are to the spatial and temporal resolution of the data sets and to methods used in the reanalysis. Typically, in LIM construction, data are first prefiltered to remove some noise that may impact the robustness of the computation; here, we prefilter SSTa to retain its leading 25 EOFs, defined within the specified region, and their corresponding principal component time series. Prior to the EOF, we also apply a 3-month running mean to the SSTa. For all the data sets considered, this reconstructed SSTa explains approximately 89% of the original variance:

$$\widehat{SSTa}\,(s,t) = \sum_{k=1}^{25} e\,(s,k)\,x\,(k,t), \qquad 5.$$

where $e(s,k)$ represents the EOF pattern for each mode k, s is the spatial coordinate, and $x(k,t) = \mathbf{x}(t)$ is the kth principal component. Furthermore, previous studies have shown that SSTa LIMs, sometimes also augmented with sea surface height information, are generally a good forecast model on subseasonal to interannual timescales and can be used to diagnose predictability, both of itself and of operational climate global circulation models (e.g., Newman 2007, 2013; Alexander et al. 2008; Newman & Sardeshmukh 2017). As a dynamical model, the LIM quantifies the impact of different processes on the system state's evolution (Newman et al. 2011).

3.2. Eigenmodes of Pacific Decadal-Scale Variability Dynamics

We now inspect the dominant low-frequency dynamical eigenmodes of Pacific SSTa, $\mathbf{u}_i$, and their temporal evolution $\alpha(t)$ ordered by their e-folding timescale. **Table 1** presents the decay timescales and periodicities of the eigenmodes computed from the different reanalysis products, including

Table 1 Eigenmodes of Pacific SSTa

HadISST (1900–2017)		HadISST (1950–2017)		NOAA ERSST v3b (1950–2019)		ORAS4 (1958–2016)		Color legend
Decay (m)	Period (year)	Decay (m)	Period (year)	Decay (m)	Period (year)	Decay (m)	Period (year)	
88.0855	Infinite	52.1307	Infinite	65.7301	Infinite	87.2685	Infinite	Mode 1: Trend
24.6269	Infinite	18.7204	22.3145	22.0524	Infinite	33.3471	Infinite	Mode 2: KOE
13.969	32.6714	13.9307	Infinite	10.8996	33.8943	13.8462	19.3029	Mode 3: NP-CP
9.066	6.7867	9.2764	4.6928	10.2467	12.0864	9.2166	13.3756	Mode 4: EP-ENSO
8.3888	2.5983	8.9778	59.8087	8.2106	2.469	7.6207	2.5306	Mode 5: CP-ENSO
7.4836	13.6005	8.4413	2.349	7.7247	4.0266	7.4727	3.5311	Mode 6: ENSO decay

This table shows the decay timescales and periods of the six dominant low-frequency LIM eigenmodes extracted from HadISST, NOAA ERSST v3b (Smith et al. 2008), and ORAS4. The modes are labeled 1–6 in the legend column and have been named based on their spatial expressions and color-coded in the table. Note that the actual order of the modes is not consistent in all of the data sets, and the modes were identified through correlation analysis of the spatial and temporal evolution of the modes across the data sets. Also, the modes with a finite period have conjugate pairs, which have been omitted from the table. Abbreviations: CP, central Pacific; ENSO, El Niño–Southern Oscillation; EP, eastern Pacific; HadISST, Hadley Centre Sea Ice and Sea Surface Temperature; KOE, Kuroshio–Oyashio Extension; LIM, linear inverse model; NOAA ERSST v3b, National Oceanic and Atmospheric Administration Extended Reconstructed Sea Surface Temperature version 3b; NP, North Pacific; ORAS4, Ocean Reanalysis System 4; SSTa, sea surface temperature anomalies.

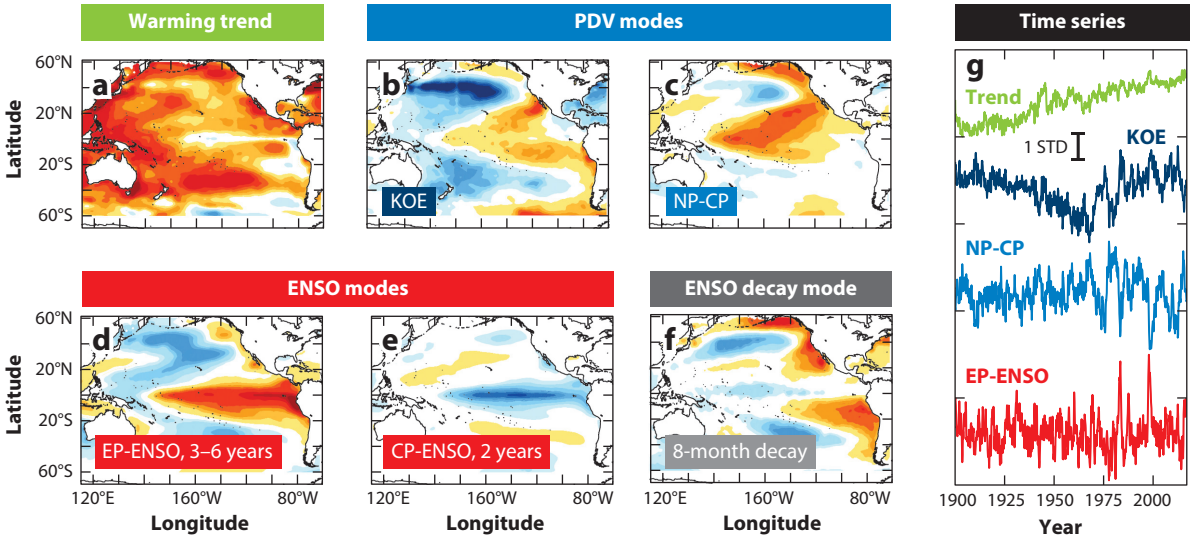

Figure 3

(*a–f*) Dynamical modes of Pacific climate, showing the ensemble average eigenmodes of the dynamical operator of LIMs developed using SSTa from the HadISST (1900–2017), NOAA ERSST v3b (1950–2019), and ORAS4 (1958–2016) data sets for the warming trend (panel *a*), two PDV modes (panels *b* and *c*), two ENSO modes (panels *d* and *e*), and the ENSO decay mode (panel *f*). (*g*) The respective normalized real-part time series derived from HadISST. The ensemble average was determined by computing the normalized spatial patterns of the modes in each data set and then averaging them together. The units are nondimensional (−1, 1), and each pattern was normalized using the standard deviation of their correspondent real-part time series prior to taking the ensemble average. Abbreviations: CP, central Pacific; ENSO, El Niño–Southern Oscillation; EP, eastern Pacific; HadISST, Hadley Centre Sea Ice and Sea Surface Temperature; KOE, Kuroshio–Oyashio Extension; LIM, linear inverse model; NOAA ERSST v3b, National Oceanic and Atmospheric Administration Extended Reconstructed Sea Surface Temperature version 3b; NP, North Pacific; ORAS4, Ocean Reanalysis System 4; PDV, Pacific decadal-scale variability; SSTa, sea surface temperature anomalies; STD, standard deviation.

an analysis of HadISST, which uses a subset of the temporal data from between 1950 and 2017 to examine the sensitivity of the modes to shorter temporal samples. After careful inspection and comparison of eigenmode structures across the data sets, we identified six robust dynamical modes, which are shown in **Figure 3** by averaging the spatial structures of the modes reconstructed in each data set.

The first mode captures the warming trend (**Figure 3*a***) over the Pacific basin and is also referred to as the least damped mode (see also Frankignoul et al. 2017) since it is a stationary (i.e., nonpropagating) eigenmode with the longest decay timescale (e.g., infinite in this case). Mode 2 captures a multidecadal timescale that has projections globally (**Figure 3*b***) and exhibits one of its centers of actions in the Kuroshio–Oyashio Extension (KOE). For the purposes of this review, we refer to this as the KOE eigenmode because some of the dynamics of this mode track the KOE global-scale teleconnections of PDV. Mode 3 has a decadal timescale and exhibits heavy loading in the North Pacific–central Pacific (NP-CP) regions (**Figure 3*c***). This recurrent pattern of PDV was recently discussed as influential for the development of northeast Pacific marine heatwaves and was termed the NP-CP eigenmode because of its centers of action (Capotondi et al. 2022). Earlier, it was identified as an important contributor both to the PDO (Newman et al. 2016) and to optimal development of ENSO anomalies (Penland & Sardeshmukh 1995, Newman et al. 2011, Capotondi et al. 2022). It captures the spatial expression of the two-way coupling between the tropics and extratropics (Di Lorenzo et al. 2015, Zhao & Di Lorenzo 2020).

Next, we identified a series of higher eigenmodes that (along with the NP-CP eigenmode) track ENSO diversity: an eastern Pacific expression (EP-ENSO) (**Figure 3*d***) with a periodicity ranging from 3 to 6 years and a central Pacific expression (CP-ENSO) (**Figure 3*e***) with a shorter biennial periodicity that is consistent across all the data sets and in agreement with the dominant observed CP-ENSO timescale (Penland & Sardeshmukh 1995, Newman et al. 2011, Capotondi et al. 2021) (see **Table 1**). The time series of these modes from HadISST, which has the longest coverage, are shown in **Figure 3*g*** and reveal the multidecadal nature of the KOE eigenmode, the decadal variability of the NP-CP eigenmode, and the interannual timescale of the EP-ENSO, with prominent peaks during the 1982 and 1997 El Niño events. We also found another robust eigenmode that emerges in all of the data sets, which we refer to here as the ENSO decay mode (**Figure 3*f***). Although this mode has not been previously described in the literature, its spatial expression is characterized by the typical projection patterns of ENSO teleconnections in the extratropics during peak El Niño events (Ashok et al. 2007, Liu & Alexander 2007, Deser et al. 2017, Wang et al. 2017), suggesting that it is linked to the adjustment dynamics of the extratropics after an ENSO perturbation. The decay timescale of this mode is approximately 8 months.

3.3. Dynamic Filtering of the Pacific Decadal-Scale Variability Modes

A close inspection of the low-frequency PDV eigenmodes that emerge from the LIM eigenanalysis reveals that the KOE and NP-CP modes very closely track the two leading global EOFs of the 8-year low-pass SSTa shown in **Figure 1**. This similarity provides further evidence that the KOE and NP-CP modes are the fundamental constituents of PDV. Indeed, we showed in Section 1 how a linear combination of the time series of the two global EOF modes can reconstruct much of the low-frequency variability of the IPO, NPGO, PDO, SPDO, and TPDV patterns (**Figure 1*e***). Here, we use an alternative approach to quantify the role of the dynamical PDV eigenmodes in contributing to the patterns of the statistical modes (i.e., the IPO, PDO, SPDO, and TPDV). We used the LIM to remove (i.e., dynamically filter) the KOE and NP-CP modes and analyzed the residual variance, following the approach originally developed by Penland & Matrosova (2006). Specifically, we reconstructed the SSTa field after removing the first three eigenmodes of Pacific SST, corresponding to the warming trend ($i = 1$), KOE ($i = 2$), and NP-CP ($i = 3$) modes, as

$$SSTa_{\text{filtered}}(s,t) = \sum_{k=1}^{25}\sum_{i=3}^{25} e(s,k)u(k,i)v^{\text{H}}(i,k)x(k,t) \qquad 6.$$

and quantified how much of the variance of the statistical modes remains in the dynamically filtered $SSTa_{\text{filtered}}$ by computing regression maps of these fields with the indices of the IPO, PDO, SPDO, and TPDV (**Figure 4**). In Equation 6, the k index refers to the EOF structures that are used to project the eigenmodes i back into physical space s. Also note that while we refer to the KOE and NP-CP modes as $i = 2$ and $i = 3$, respectively, all of these are propagating modes that come as conjugate pairs that need to be filtered out together. With just these three PDV eigenmodes removed, the IPO standard deviation spatial structure is reduced to almost zero loading throughout the basin (**Figure 4**). For the TPDV pattern, the basin-scale and central tropical Pacific loadings are also significantly reduced, with most of the residual decadal variance in the tropical Pacific found in a narrow, tropically confined EP-ENSO expression. In the case of the PDO and SPDO patterns, a strong EP-ENSO expression emerges in the filtered SSTa, consistent with previous studies showing that ENSO is a key dynamical process contributing to the interannual power of these climate indices (e.g., Newman et al. 2016).

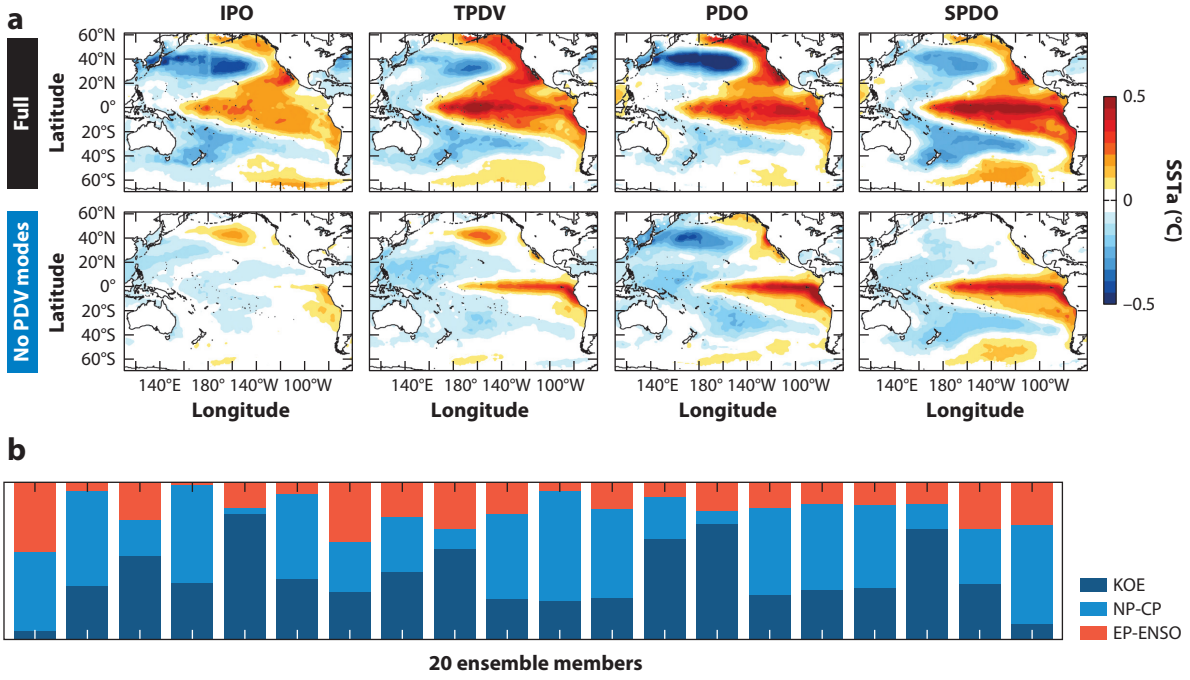

Figure 4

Dynamical filtering of the PDV modes. (*a*) Regression maps of indices of Pacific climate variability with the SSTa from the HadISST data set (1900–2017) (*top*) and with dynamically filtered SSTa where the KOE and NP-CP modes (i.e., PDV modes) have been removed using the LIM as a dynamical filter (*bottom*). (*b*) An ensemble reconstruction of the PDO from 20 LIM stochastic simulations, showing the relative contributions of the KOE, NP-CP, and EP-ENSO eigenmodes. Abbreviations: CP, central Pacific; ENSO, El Niño–Southern Oscillation; EP, eastern Pacific; HadISST, Hadley Centre Sea Ice and Sea Surface Temperature; IPO, Interdecadal Pacific Oscillation; KOE, Kuroshio–Oyashio Extension; LIM, linear inverse model; NP, North Pacific; PDO, Pacific Decadal Oscillation; PDV, Pacific decadal-scale variability; SPDO, South Pacific Decadal Oscillation; SSTa, sea surface temperature anomalies; TPDV, tropical Pacific decadal-scale variability.

3.4. A Linear Inverse Modeling Climate Diagnostic Toolbox for Pacific Decadal-Scale Variability

While these eigenmodes emerge as the fundamental constituents of PDV, the relative importance of each eigenmode in explaining the patterns of the IPO, PDO, and SPDO can change due to internal noise and external forcing of the Pacific climate system. For example, using a stochastic numerical integration of the LIM (Equation 2) with different realizations of white noise $\boldsymbol{\xi}(t)$ derived from the spatial structure of the noise covariance matrix $\langle \boldsymbol{\xi}\boldsymbol{\xi}^{\mathrm{T}} \rangle \mathrm{d}t = -(\mathbf{L}\mathbf{C}_0 + \mathbf{C}_0\mathbf{L})$, we can easily generate $O(10{,}000)$ years of SSTa, spanning the phase space of SST evolution more completely than more limited and computationally expensive Earth system model ensembles (methods described in Penland & Matrosova 1994). Even within the same unforced world, there can be significant internal variability in the character and dynamical constituents of climate patterns like the PDO from one 60-year period to the next (**Figure 4**; the reconstruction approach is explained in Newman et al. 2016). For example, some realizations show that the PDO variance is dominated by the EP-ENSO, while in others, the KOE or NP-CP becomes more dominant, including extremes where one of the mode's expression is almost absent. Quantifying and understanding this range is key for comparing the PDV processes across Earth system models (Furtado et al. 2011, Zhao et al. 2021a). As part of this review, we are also releasing the LIM Climate Diagnostic Toolbox

for PDV (**http://pdv-tools.org**), which was used to compute the data shown in the figures in this review (e.g., the eigenmode decomposition in **Figure 3** and the dynamic filtering and stochastic simulation in **Figure 4**), to allow future studies to examine and compare the PDV modes across different observational and Earth system model data sets.

4. MECHANISMS ENERGIZING THE PACIFIC DECADAL-SCALE VARIABILITY MODES

In Section 3, we identified that the fundamental dynamical constituents of PDV are linked to the KOE and NP-CP modes (**Figure 3*b*,*c***). We now explore the mechanisms that are important for supporting the spatial and temporal evolution of these dynamical modes.

4.1. Tropical Pacific Decadal-Scale Variability and Extratropical ENSO Precursors

Both PDV modes (i.e., KOE and NP-CP) show that the interactions between the extratropics and the tropical Pacific play a dominant role in the basin-scale low-frequency variability. Therefore, we introduce the relevant Pacific-wide teleconnections that are mediated by the tropical Pacific and that are important for energizing and synchronizing the basin-scale PDV. We have reviewed how the spatial pattern of TPDV (**Figure 4**) extends beyond the tropical Pacific with a clear basin-scale pattern. The primary mechanisms by which the tropical variance is exported over the Pacific basin are the ENSO teleconnections to the extratropics via atmospheric Rossby waves (e.g., the atmospheric bridge) (Hoskins & Karoly 1981, Sardeshmukh & Hoskins 1988, Alexander et al. 2002, Taschetto et al. 2020) and oceanic Kelvin waves (Schwing et al. 2002) along the eastern boundaries. Both teleconnection mechanisms are strongest in the boreal fall and winter, when the ENSO cycle is at its peak. Their projections on the North and South Pacific energize the basin-scale pattern of TPDV (**Figure 5**; the oceanic teleconnections are not represented in this schematic, and their impacts are more confined to the boundaries). While these one-way teleconnections out of the tropics have been widely documented (see also Hoerling et al. 1997, Deser et al. 2004), recent studies suggest that a two-way coupling between tropics and extratropics associated with ENSO extratropical precursors is critical for explaining PDV (Di Lorenzo et al. 2015, Stuecker 2018, Zhao & Di Lorenzo 2020, Lou et al. 2021).

Extratropical ENSO precursor dynamics are activated by anomalies in the off-equatorial trade winds in both the South and North Pacific. The first precursors are the meridional modes (Chiang & Vimont 2004, Zhang et al. 2014). First described in the context of the North Pacific seasonal footprinting mechanism (Vimont et al. 2001, 2003), the meridional modes are associated with a reduction in the off-equatorial trades that, through the so-called wind–evaporation–SST thermodynamic feedback (Xie 1999), result in coupled ocean–atmosphere anomalies that propagate into the tropics during their growth cycle and favor ENSO conditions (Vimont et al. 2009, Vimont 2010, Martinez-Villalobos & Vimont 2017). Meridional modes have been documented from both the North Pacific (Chiang & Vimont 2004, Chang et al. 2007) and South Pacific (Zhang et al. 2014), appearing to act independently between the two hemispheres (Ding et al. 2015, 2017; Min et al. 2017) (**Figure 5**) and potentially contributing to different types of ENSO-like variability (Anderson et al. 2013a, Vimont et al. 2014, Meehl et al. 2017, You & Furtado 2018, Liguori & Di Lorenzo 2019). A second type of extratropical ENSO precursor is linked to modulations in the strength of the subtropical cells (Capotondi et al. 2005) and meridional heat transport into the equatorial thermocline (Anderson 2007)—a mechanism termed the trade wind–induced charging (Anderson et al. 2013b, Anderson & Perez 2015). The last type of ENSO precursor is linked to the trade wind excitation of off-equatorial Rossby waves (Knutson & Manabe 1998), which

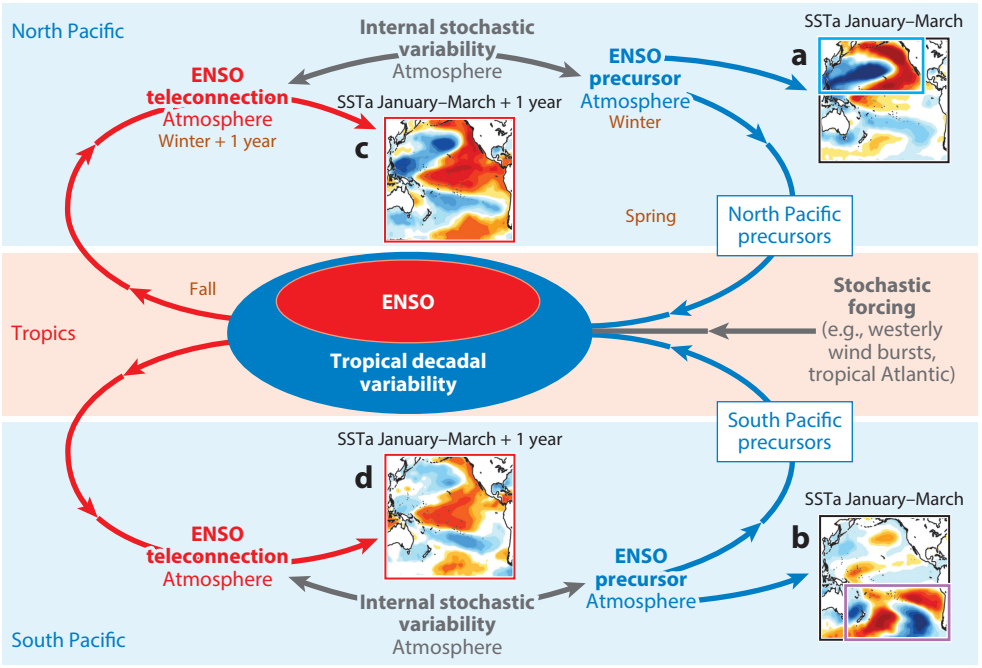

Figure 5

Null hypothesis for energizing the basin-scale tropically symmetric PDV pattern. The gray path shows how high-frequency stochastic variabilities in the atmosphere influence the ENSO systems. The blue path shows the growing phase of the TPDV, which is the sequence ENSO precursors (extratropics) → ENSO (tropics). The red path shows the decaying phase of the TPDV, which is the sequence ENSO (tropics) → ENSO teleconnections (extratropics). The SSTa maps in the North Pacific and South Pacific regions represent the oceanic expressions of the northern and southern ENSO precursors, respectively, in January–March (panels *a* and *b*) and their seasonal progression in January–March +1 (panels *c* and *d*). These maps were obtained by correlating the ENSO seasonal precursors and teleconnection indices with SSTa. Abbreviations: ENSO, El Niño–Southern Oscillation; PDV, Pacific decadal-scale variability; SSTa, sea surface temperature anomalies; TPDV, tropical Pacific decadal-scale variability. Figure adapted from Zhao & Di Lorenzo (2020) (CC BY 4.0).

propagate thermocline anomalies to the equatorial western boundary. The reflection of these waves as eastward Kelvin waves along the equator is known to trigger ENSO feedbacks by modulating upwelling (e.g., the thermocline feedback) [see review by Wang (2018)].

The dynamic sequence initiated by ENSO precursors (extratropics) → ENSO (tropics) → ENSO teleconnections (extratropics) (summarized in **Figure 5**) has been proposed as a fundamental null-hypothesis mechanism for reddening Pacific stochastic perturbations into the pattern of PDV (Di Lorenzo et al. 2015) (e.g., **Figure 1*d***). More specifically, Zhao & Di Lorenzo (2020) illustrated that independent stochastic seasonal forcings of the North and South Pacific extratropical precursors, which show different patterns in the SSTa (**Figure 5*a***, e.g., the NPMM and NPGO; **Figure 5*b***, the SPMM), are integrated through this sequence into successor patterns (**Figure 5*c*,*d***), which now exhibit the same tropically symmetric structure of the PDV pattern. In summary, this mechanism allows transferring stochastic variability from one hemisphere to the other through the ENSO bridge and projecting onto the canonical structure of the PDV pattern. This sequence mostly explains the meridional hemispherically symmetric fraction of PDV that is connected to the ENSO bridge and captures a large fraction of the TPDV in observations (~65%) and climate models (Zhao & Di Lorenzo 2020, Zhao et al. 2021a). However, TPDV has

important contributions from several other sources internal to the tropics, including stochastic forcing, such as westerly wind bursts (**Figure 5**), teleconnections with the tropical Atlantic, and anthropogenic forcing [see review by Power et al. (2021)]. These sources also contribute to reddening the extratropics through ENSO teleconnections.

4.2. The North Pacific–Central Pacific Mode: Two-Way Coupling Between Tropics and Extratropics

Building on the two-way coupling dynamics between the tropical and extratropical Pacific, we now examine in more depth the dynamics of the NP-CP eigenmode (**Figure 3*c***) and its contribution to the statistical patterns of variance of the known Pacific climate modes. We begin by noting that the nature of oceanic and atmospheric ENSO teleconnections from the tropics to the extratropics may depend on ENSO diversity (Capotondi et al. 2015). For example, the EP-ENSO teleconnections energize the AL and PDO patterns in the North Pacific on seasonal to interannual timescales (Newman et al. 2003, Schneider & Cornuelle 2005, Vimont 2005) through the atmospheric bridge (Alexander et al. 2002) (**Figure 6*a***, arrow ①) and project onto the spatial expression of the SPDO in the South Pacific (Chen & Wallace 2015, Lou et al. 2019). Similarly, tropical atmospheric teleconnections associated with the CP-ENSO energize the NPO (atmosphere) and NPGO (ocean) patterns (Di Lorenzo et al. 2010) (**Figure 6*a***, arrow ②) and act on the PDO on somewhat longer timescales (Newman et al. 2016, Zhao et al. 2021b).

In the North Pacific, NPO variability is linked to anomalous off-equatorial trade winds, activating the extratropical precursor dynamics discussed in Section 4.1 (e.g., Knutson & Manabe 1998, Vimont et al. 2001, Anderson 2003, Anderson et al. 2013b) (**Figure 6*a***, arrow ③). We hypothesize that the linkages captured by the sequence NPO/NPGO/NPMM (extratropics) → CP-ENSO (tropics) → NPO/NPGO/NPMM (extratropics) (Furtado et al. 2012, Stuecker 2018) are connected to the dynamics driving the evolution of the NP-CP eigenmode. In fact, recent studies

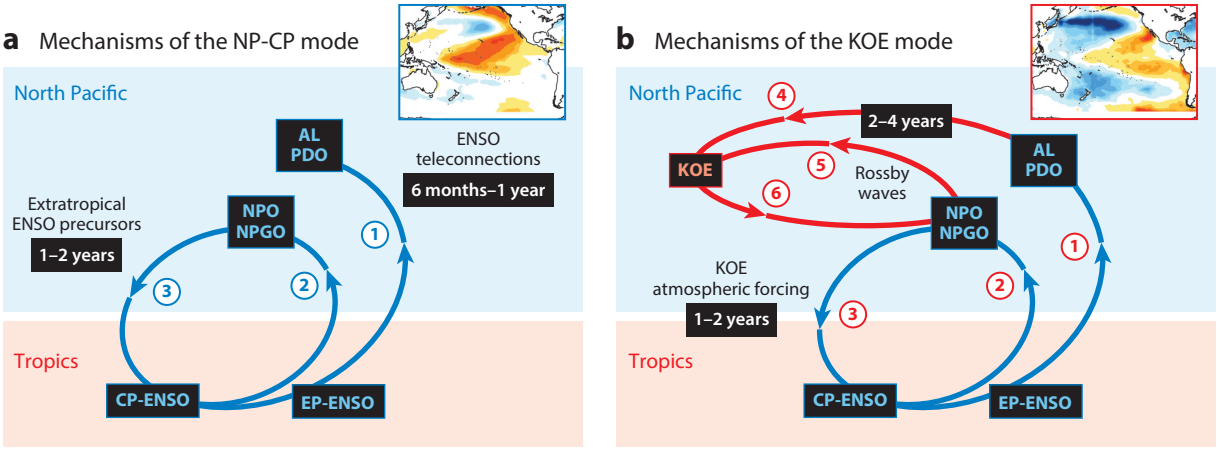

Figure 6

Mechanisms of the NP-CP and KOE modes. The NP-CP mode (panel *a*) is energized by the two-way coupling dynamics between the tropics and extratropics. The KOE mode (panel *b*) is energized by the two-way coupling between the KOE and the central and eastern North Pacific and its interactions with the NP-CP mode. The color maps in the top right corner of each panel show the spatial expression of the modes from **Figure 3**. Abbreviations: AL, Aleutian Low; CP, central Pacific; ENSO, El Niño–Southern Oscillation; EP, eastern Pacific; KOE, Kuroshio–Oyashio Extension; NP, North Pacific; NPGO, North Pacific Gyre Oscillation; NPO, North Pacific Oscillation; PDO, Pacific Decadal Oscillation.

suggest that this two-way coupling between the tropical Pacific and the North Pacific is an important mechanism for supporting multiyear ENSO (Ding et al. 2022) via the sequence NPO → CP-ENSO → NPO → CP-ENSO (**Figure 6*a***, loop ③–②). Note that to the extent that these dynamics are represented by the NP-CP eigenmode, its roughly one-year memory timescale limits the predictability of this coupling process. Furthermore, given that the NPO precedes both the CP- and EP-ENSO flavors, the teleconnection sequence NPO/NPGO → EP-ENSO → AL/PDO has been invoked as a key mechanism for explaining the one-year lag correlation between the expressions of the NPGO and PDO (Joh & Di Lorenzo 2017) and the persistence of multiyear climate extremes of the North Pacific such as the 2013–2015 marine heatwaves and droughts over North America (Anderson et al. 2016, Di Lorenzo & Mantua 2016, Capotondi et al. 2019, Xu et al. 2021). Other studies show that the NP-CP eigenmode may be impacted by climate change, as the links between the NPO and the tropics could be intensifying under greenhouse warming (Liguori & Di Lorenzo 2018) and thereby enhancing ENSO variability and amplitude (Jia et al. 2021).

4.3. The Kuroshio–Oyashio Extension Mode: Coupling Between the Kuroshio–Oyashio Extension and Pacific Climate

Turning to the KOE eigenmode (**Figure 3*b***), we first note that the characteristic pattern of this mode has substantial similarity to that of the NP-CP eigenmode, even though it exhibits higher loading in the KOE and South Pacific. This is again a consequence of the nonorthogonality of the dynamical eigenmodes. Indeed, despite the independence of the KOE and NP-CP modes, their time series are significantly correlated ($R = 0.61$, >95% significance) (**Figure 3*g***), partly due to the spatial structure of their noise forcing. In other words, these eigenmodes evolve separately on seasonal to decadal timescales but could still be linked by much faster dynamical processes, which in the LIM are approximated as white noise. To understand how the interference between these two modes contributes to PDV, we first review the large-scale climate teleconnections to and from the KOE. The oceanic adjustment of sea surface height anomalies to North Pacific basin atmospheric forcing (e.g., the AL) excites long oceanic Rossby waves that propagate into the KOE region on timescales of 2–4 years (Schneider & Miller 2001, Qiu 2003, Sasaki & Schneider 2011) (**Figure 6*b***, arrow ④), which contribute to the PDO signal there (Newman et al. 2016). The arrival of these waves exerts a primary control on the low-frequency meridional displacement of the KOE axis (Taguchi et al. 2007). Similarly, the NPGO sea surface height anomalies propagate to the western boundary and drive low-frequency changes that project onto modulations in the KOE circulation strength (Ceballos et al. 2009, Anderson 2019) (**Figure 6*b***, arrow ⑤). Together, the fluctuations of the KOE axis and intensity capture more than 60% of the western North Pacific PDV. Moreover, they are linked to changes in the mesoscale structure of the KOE (Qiu & Chen 2005, Qiu et al. 2014), which may have important implications for large-scale air–sea interactions [see review by Kwon et al. (2010)]. Given that a fraction of the variability of the PDO and NPGO patterns is linked to the tropical Pacific (**Figure 6*b***, arrows ①–③), the lagged ocean wave teleconnection to the KOE provides a mechanism for explaining the basin-scale expression of the KOE eigenmode in the tropical Pacific.

While large-scale processes drive the low-frequency variability of the KOE, the KOE in turn can drive large-scale atmospheric teleconnections that impact basin-scale variability. For example, several observationally based studies use lead/lag statistics between the KOE and the North Pacific atmosphere to suggest that low-frequency changes in the KOE can feed back into Pacific climate by triggering downstream atmospheric teleconnections in the central and eastern North Pacific (Frankignoul et al. 2011, Qiu et al. 2014, Na et al. 2018, Anderson 2019). Specifically, decadal changes in KOE oceanic forcing associated with oceanic heat content variability and changes in

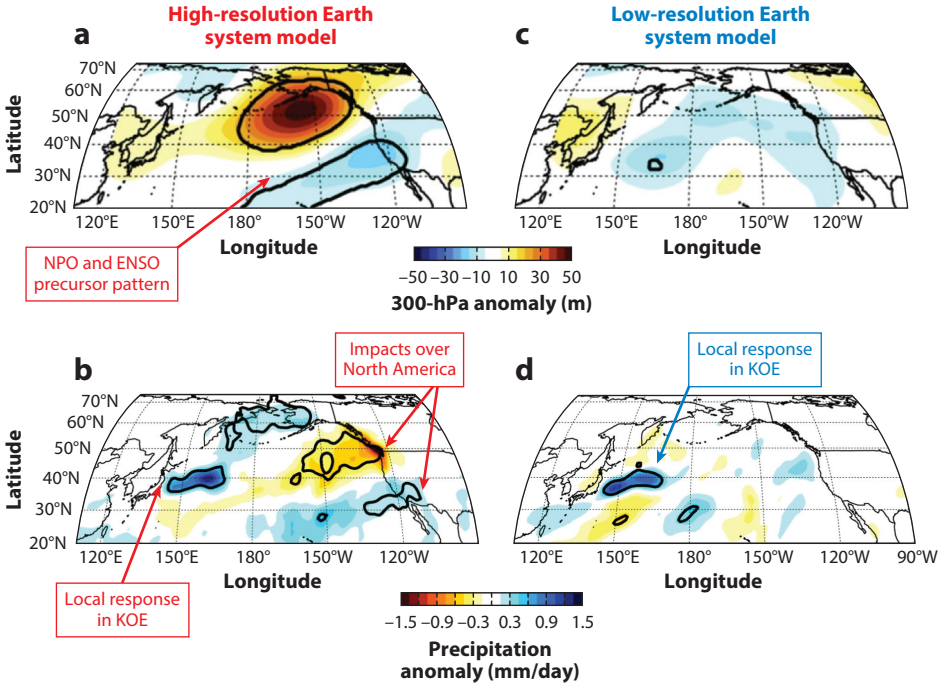

Figure 7

Atmospheric response to KOE SSTa frontal variability in Earth system model ensembles. Panels *a* and *b* show the responses of the 300-hPa and precipitation anomalies, respectively, in high-resolution (∼25-km) ensemble simulations, and panels *c* and *d* show the responses in low-resolution (∼100-km) ensemble simulations. In the high-resolution simulations, the KOE-induced atmospheric response strongly projects onto the NPO and North Pacific ENSO precursor patterns (panel *a*) and significantly impacts precipitation over North America (panel *b*). Black contours denote areas that are significant at the 95% level. Abbreviations: ENSO, El Niño–Southern Oscillation; KOE, Kuroshio–Oyashio Extension; NPO, North Pacific Oscillation; SSTa, sea surface temperature anomalies. Figure adapted with permission from Smirnov et al. (2015).

gyre circulations possibly alter the position and intensity of the atmospheric boundary layer (e.g., extratropical storm track) and drive the corresponding atmospheric response over the North Pacific. The reported downstream atmospheric response pattern to the Kuroshio decadal changes reveals a strong consistency across different oceanic variables of the KOE (summarized in figure 2 in Joh & Di Lorenzo 2019). These feedback dynamics have been reproduced in some coupled ocean–atmosphere model experiments with sufficiently high resolution to resolve mesoscale air–sea coupling in the KOE (**Figure 7*a***) and are linked to significant changes in precipitation over North America (Smirnov et al. 2015, Ma et al. 2017, Siqueira et al. 2021) (**Figure 7*b***).

The dynamics associated with the two-way coupling in the North Pacific between the KOE and the central and eastern North Pacific (**Figure 6*b***, arrows ④–⑥) could energize preferred decadal timescales of variability (Qiu 2003; Qiu et al. 2007, 2014) and may also be linked to a quasi-decadal progression of atmospheric pressure anomalies and SSTa around the North Pacific termed the Pacific Decadal Precession (Anderson et al. 2016, 2017; Anderson 2019). A closer examination of the sea level pressure, wind stress curl, and Ekman pumping anomalies driven by the KOE atmospheric downstream response reveals that these anomalies have a strong projection on the NPO (**Figure 7*a***) and the region of excitation of the North Pacific ENSO precursors (e.g., the

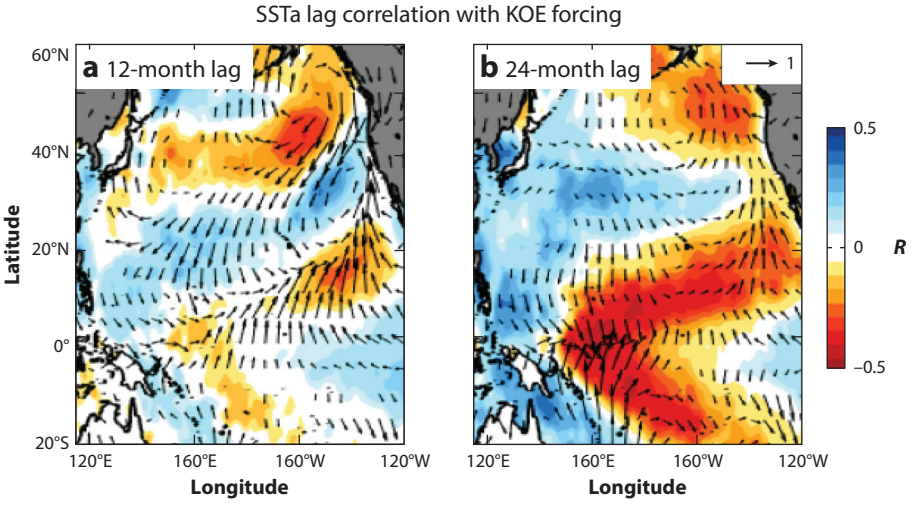

Figure 8

Averaged correlation maps of wind stress and SSTa response to a KOE forcing index for lags of (*a*) 12 months and (*b*) 24 months. Abbreviations: KOE, Kuroshio–Oyashio Extension; SSTa, sea surface temperature anomalies. Figure adapted from Joh & Di Lorenzo (2019) (CC BY 4.0).

seasonal footprinting mechanism). Using observational and modeling approaches, recent studies have shown that these downstream teleconnection dynamics can in fact impact the CP-ENSO by activating the North Pacific ENSO precursors (Joh & Di Lorenzo 2019, Joh et al. 2021), which may mean that they optimally initiate the NP-CP eigenmode (Capotondi et al. 2022). Specifically, the atmospheric response to the low-frequency oceanic forcing of the KOE acts as a nudging of the NPO conditions on timescales of 1–2 years and energizes the sequence KOE → NPO → CP-ENSO → NPO/NPGO → KOE (**Figure *6b***, arrows ⑥, ③, ②, and ⑤). This sequence better explains the quasi-decadal timescale of the KOE/CP-ENSO spectrum that is also reported in long-term paleo-proxy observations (Nurhati et al. 2011).

To better visualize the coupling between the KOE and NP-CP modes, we examine the evolution of the KOE-driven forcing sequence KOE → NPO → CP-ENSO discussed by Joh & Di Lorenzo (2019). **Figure 8** shows the time-lag spatial evolutions of the SSTa and wind response to KOE forcing at lags of 12 and 24 months (for details, see Joh & Di Lorenzo 2019). The signal from the KOE and North Pacific progresses into the central tropical Pacific. This progression mechanism linking the KOE to the CP-ENSO has been preliminarily confirmed in a high-resolution ocean–atmosphere model and in LIM simulations (Joh et al. 2021), with indications that anthropogenic climate change may be intensifying the KOE teleconnections to PDV and the CP-ENSO. Further evidence supporting the important role of these coupling dynamics comes from a recent study showing that if we decouple the North Pacific and tropical Pacific in the LIM framework, the North Pacific climate variability (e.g., the PDO pattern) is dominated by strong loading in the KOE, with a substantial loss of variance in the North Pacific expression of the NP-CP mode (Zhao et al. 2021b).

So far, we have discussed the KOE eigenmode in terms of its two-way teleconnections with the North Pacific and tropical Pacific. However, this eigenmode also has a clear expression in the South Pacific. While this expression is explained partly by the reddening of the KOE forcing through its connections to the ENSO system, the South Pacific can also act as a forcing of this pattern through the ENSO bridge on low-frequency timescales (Garreaud & Battisti 1999).

We have already discussed that the SPMM dynamics triggered by the SPO wind anomalies can energize the ENSO system and TPDV pattern. Some studies suggest that the SPMM has stronger influences on the tropical Pacific on decadal versus interannual timescales. Sensitivity simulations with an ensemble of coupled climate models suggest that while the NPMM energizes the CP-ENSO pattern on interannual timescales, the SPMM energizes the decadal variance of the EP-ENSO (Liguori & Di Lorenzo 2019). Furthermore, other studies have pointed out that the off-equatorial winds from the South Pacific also have a direct path to the eastern tropical Pacific and can lead to ocean low-frequency variance through a simple integration (i.e., the AR-1 model shown in Equation 1) of the atmospheric variability (Okumura 2013). Collectively, these processes from the South Pacific may energize the KOE eigenmode.

5. SUMMARY AND CONCLUSIONS

This review has highlighted evidence for a modified paradigm of the interactions of various modes of PDV and how the important mechanisms at play in the ocean–atmosphere system basin-wide may yield this variability. The dominant statistical modes of basin-scale PDV, such as the IPO and TPDV, are linked and explain a large fraction of the global low-frequency variability in SSTa (Section 2; **Figure 1**). The extratropical SSTa patterns of PDV over the North and South Pacific, variously defined as the PDO, SPDO, NPGO, NPMM, and SPMM, are also linked to the global SSTa decadal-scale variability. Their patterns can be explained to first order by a reddening of the atmospheric forcing that arises from a shift and/or intensification and weakening of the atmospheric mean circulation's pressure systems (Section 2.1; **Figure 2**). At low frequencies, all statistical modes of Pacific climate converge to an ENSO-like pattern of TPDV (Section 2.2), highlighting the important role of ENSO dynamics as a bridge to establish the basin-scale PDV.

While the description of PDV from the statistical modes is useful to track the state of Pacific climate and its impacts on weather and marine ecosystems, it does not explicitly resolve the dynamics of atmospheric and oceanic teleconnections or the coupled feedbacks, which are important for understanding PDV. For this reason, we used the LIM Climate Diagnostic Toolbox for PDV (developed for this review and available at **http://pdv-tools.org**) to empirically reconstruct the dynamical operator of Pacific climate and its eigenmodes using a reduced observation space (Section 3.1). After extracting the leading LIM eigenmodes from three reanalysis products—HadISST, NOAA ERSST v3b, and ORAS4 (Sections 3.2 and 3.3; **Figure 3**; **Table 1**)—we showed that the spatial patterns of variance of PDV (e.g., the IPO, PDO, and TPDV) result from the interaction of the two lowest-frequency dynamical eigenmodes, the KOE and NP-CP eigenmodes (**Figure 4**). The spatial structure of these two eigenmodes is basin-scale and depicts that two-way teleconnection dynamics between the tropics and extratropics associated with the sequence ENSO precursors (extratropics) → ENSO (tropics) → ENSO teleconnections (extratropics) (Section 4.1; **Figure 5**) are the fundamental mechanisms to energize and synchronize the basin-scale footprint of PDV. More specifically, the NP-CP eigenmode captures interannual- to decadal-scale variability and energizes the variance of the NPO/NPGO (extratropics) → CP-ENSO (tropics) → NPO/NPGO (extratropics) sequence (Section 4.2; **Figure 6**). The KOE eigenmode exhibits a basin-scale structure that resembles the IPO and is characterized by decadal to multidecadal timescales. It tracks the two-way teleconnections of the KOE with the central and eastern North Pacific associated with the propagation of Rossby ocean waves into the KOE and the air–sea feedback response of the KOE onto the downstream atmospheric circulation of the North Pacific. This downstream response couples the KOE eigenmode to the NP-CP by activating the ENSO extratropical precursors and leads to a multiannual preferred timescale of variability linked to the sequence KOE → NPO → CP-ENSO → NPO/NPGO → KOE (Section 4.3; **Figure 6**).

Although the NP-CP mode emerges as an oscillatory eigenmode, its period is much longer than its decay timescale (**Table 1**). This implies that it is unlikely that a sustained oscillation of this eigenmode will ever be observed. Therefore, while the eigenmode captures the dynamical sequences summarized here, these sequences will only be predictable over some finite period until they eventually become entirely obscured by noise events that are largely unpredictable.

While this synthesis has highlighted some of the dynamical modes and mechanisms of PDV across various reanalysis products, we must recognize that these observational sources are still relatively short in total period of record, which introduces some uncertainties in our ability to cleanly resolve the modes and diagnose their mechanisms. It also remains unclear how nonstationarity in the data and in the projections for future climate influences the expression of the dynamical modes. Furthermore, we have shown through stochastic simulations of the LIM (Section 3.4) that different realizations of Pacific climate from the same dynamical operator can lead to substantial differences in the relative importance that each mode plays in explaining the statistical patterns of PDV, such as the PDO. Acknowledging and quantifying this range of uncertainty is critical for analyzing and comparing Earth system models and assessing the significance of changes in the PDV dynamics related to anthropogenic forcing, which we have not addressed in this review. Future studies may want to use the LIM diagnostic approach to explore PDV in a changing climate.

DISCLOSURE STATEMENT

The authors are not aware of any affiliations, memberships, funding, or financial holdings that might be perceived as affecting the objectivity of this review.

AUTHOR CONTRIBUTIONS

E.D.L. conceived and wrote the article and designed the figures. T.X. contributed the LIM Climate Diagnostic Toolbox; M.N. helped structure the article and made key contributions to Section 3; S.W. contributed the climate model analysis in Section 3.3; Y.Z. contributed to the writing of Section 4.1; and Y.J., A.C., R.D., and G.N. contributed to the writing of Sections 4.2 and 4.3. The other authors provided content on the following areas: S.S. on ENSO and tropical climate; D.J.A., B.T.A., G.L., and D.J.V. on North Pacific ENSO precursors; J.C.F., J.L., and H.Z. on South Pacific ENSO precursors; B.T.A., Y.J., and N.S. on KOE teleconnections, and A.J.M. on the motivation and scope of the article. All authors participated in developing the structure of the article and in editing and revisions.

ACKNOWLEDGMENTS

This research and synthesis work was supported primarily by the US Department of Energy's Regional and Global Model Analysis program (grant DE-SC0019418). E.D.L. and A.J.M. were partly supported by the National Science Foundation (grants OCE-1948627 and OCE-2022868, respectively). A.C. was supported by the NOAA Climate Program Office Climate Variability and Predictability program.

LITERATURE CITED

Alexander MA. 2010. Extratropical air-sea interaction, SST variability and the Pacific Decadal Oscillation (PDO). In *Climate Dynamics: Why Does Climate Vary?*, ed. D-Z Sun, F Bryan, pp. 123–48. Washington, DC: Am. Geophys. Union

Alexander MA, Blade I, Newman M, Lanzante JR, Lau NC, Scott JD. 2002. The atmospheric bridge: the influence of ENSO teleconnections on air-sea interaction over the global oceans. *J. Clim.* 15:2205–31

Alexander MA, Matrosova L, Penland C, Scott JD, Chang P. 2008. Forecasting Pacific SSTs: linear inverse model predictions of the PDO. *J. Clim.* 21:385–402

Amaya DJ. 2019. The Pacific Meridional Mode and ENSO: a review. *Curr. Clim. Change Rep.* 5:296–307

Amaya DJ, Bond N, Miller AJ, DeFlorio M. 2016. The evolution and known atmospheric forcing mechanisms behind the 2013–2015 North Pacific warm anomalies. *US CLIVAR Variations*, Spring, pp. 1–6

Anderson BT. 2003. Tropical Pacific sea-surface temperatures and preceding sea level pressure anomalies in the subtropical North Pacific. *J. Geophys. Res. Atmos.* 108:4732

Anderson BT. 2007. On the joint role of subtropical atmospheric variability and equatorial subsurface heat content anomalies in initiating the onset of ENSO events. *J. Clim.* 20:1593–99

Anderson BT. 2019. Empirical evidence linking the Pacific decadal precession to Kuroshio Extension variability. *J. Geophys. Res. Atmos.* 124:12845–63

Anderson BT, Furtado JC, Cobb KM, Di Lorenzo E. 2013a. Extratropical forcing of El Niño–Southern Oscillation asymmetry. *Geophys. Res. Lett.* 40:4916–21

Anderson BT, Furtado JC, Di Lorenzo E, Gianotti DJS. 2017. Tracking the Pacific Decadal Precession. *J. Geophys. Res. Atmos.* 122:3214–27

Anderson BT, Gianotti DJS, Furtado JC, Di Lorenzo E. 2016. A decadal precession of atmospheric pressures over the North Pacific. *Geophys. Res. Lett.* 43:3921–27

Anderson BT, Perez RC. 2015. ENSO and non-ENSO induced charging and discharging of the equatorial Pacific. *Clim. Dyn.* 45:2309–27

Anderson BT, Perez RC, Karspeck A. 2013b. Triggering of El Niño onset through trade wind-induced charging of the equatorial Pacific. *Geophys. Res. Lett.* 40:1212–16

Ashok K, Behera SK, Rao SA, Weng H, Yamagata T. 2007. El Niño Modoki and its possible teleconnection. *J. Geophys. Res. Oceans* 112:C11007

Balmaseda MA, Mogensen K, Weaver AT. 2013. Evaluation of the ECMWF ocean reanalysis system ORAS4. *Q. J. R. Meteorol. Soc.* 139:1132–61

Bjerknes J. 1968. *Atmospheric teleconnections from the equatorial Pacific*. Rep., RAND Corp., Santa Monica, CA

Bograd SJ, Kang S, Di Lorenzo E, Horii T, Katugin ON, et al. 2019. Developing a social-ecological-environmental system framework to address climate change impacts in the North Pacific. *Front. Mar. Sci.* 6:333

Bond NA, Overland JE, Spillane M, Stabeno P. 2003. Recent shifts in the state of the North Pacific. *Geophys. Res. Lett.* 30:2183

Capotondi A, Alexander MA, Deser C, McPhaden MJ. 2005. Anatomy and decadal evolution of the Pacific Subtropical-Tropical Cells (STCs). *J. Clim.* 18:3739–58

Capotondi A, Newman M, Xu T, Di Lorenzo E. 2022. An optimal precursor of Northeast Pacific marine heatwaves and Central Pacific El Niño events. *Geophys. Res. Lett.* 49:e2021GL097350

Capotondi A, Ricciardulli L. 2021. The influence of Pacific winds on ENSO diversity. *Sci. Rep.* 11:18672

Capotondi A, Sardeshmukh PD. 2017. Is El Niño really changing? *Geophys. Res. Lett.* 44:8548–56

Capotondi A, Sardeshmukh PD, Di Lorenzo E, Subramanian AC, Miller AJ. 2019. Predictability of US West Coast ocean temperatures is not solely due to ENSO. *Sci. Rep.* 9:10993

Capotondi A, Wittenberg AT, Kug J-S, Takahashi K, McPhaden MJ. 2021. ENSO diversity. In *El Niño Southern Oscillation in a Changing Climate*, ed. A Santoso, M McPhaden, W Cai, pp. 65–86. Washington, DC: Am. Geophys. Union

Capotondi A, Wittenberg AT, Newman M, Di Lorenzo E, Yu JY, et al. 2015. Understanding ENSO diversity. *Bull. Am. Meteorol. Soc.* 96:921–38

Ceballos LI, Di Lorenzo E, Hoyos CD, Schneider N, Taguchi B. 2009. North Pacific Gyre Oscillation synchronizes climate fluctuations in the eastern and western boundary systems. *J. Clim.* 22:5163–74

Chang P, Zhang L, Saravanan R, Vimont DJ, Chiang JCH, et al. 2007. Pacific Meridional Mode and El Niño–Southern Oscillation. *Geophys. Res. Lett.* 34:L16608

Chen XY, Wallace JM. 2015. ENSO-like variability: 1900–2013. *J. Clim.* 28:9623–41

Chhak KC, Di Lorenzo E, Schneider N, Cummins PF. 2009. Forcing of low-frequency ocean variability in the northeast Pacific. *J. Clim.* 22:1255–76

Chiang JCH, Vimont DJ. 2004. Analogous Pacific and Atlantic meridional modes of tropical atmosphere-ocean variability. *J. Clim.* 17:4143–58

Chu PS, Clark JD. 1999. Decadal variations of tropical cyclone activity over the central North Pacific. *Bull. Am. Meteorol. Soc.* 80:1875–81

Dai AG. 2013. The influence of the inter-decadal Pacific oscillation on US precipitation during 1923–2010. *Clim. Dyn.* 41:633–46

Deepa JS, Gnanaseelan C, Mohapatra S, Chowdary JS, Karmakar A, et al. 2019. The tropical Indian Ocean decadal sea level response to the Pacific Decadal Oscillation forcing. *Clim. Dyn.* 52:5045–58

Deser C, Alexander MA, Timlin MS. 2003. Understanding the persistence of sea surface temperature anomalies in midlatitudes. *J. Clim.* 16:57–72

Deser C, Alexander MA, Xie SP, Phillips AS. 2010. Sea surface temperature variability: patterns and mechanisms. *Annu. Rev. Mar. Sci.* 2:115–43

Deser C, Phillips AS, Hurrell JW. 2004. Pacific interdecadal climate variability: linkages between the tropics and the North Pacific during boreal winter since 1900. *J. Clim.* 17:3109–24

Deser C, Simpson IR, McKinnon KA, Phillips AS. 2017. The Northern Hemisphere extratropical atmospheric circulation response to ENSO: How well do we know it and how do we evaluate models accordingly? *J. Clim.* 30:5059–82

Di Lorenzo E, Cobb KM, Furtado JC, Schneider N, Anderson BT, et al. 2010. Central Pacific El Niño and decadal climate change in the North Pacific Ocean. *Nat. Geosci.* 3:762–65

Di Lorenzo E, Combes V, Keister JE, Strub PT, Thomas AC, et al. 2013. Synthesis of Pacific Ocean climate and ecosystem dynamics. *Oceanography* 26(4):68–81

Di Lorenzo E, Liguori G, Schneider N, Furtado JC, Anderson BT, Alexander MA. 2015. ENSO and meridional modes: a null hypothesis for Pacific climate variability. *Geophys. Res. Lett.* 42:9440–48

Di Lorenzo E, Mantua N. 2016. Multi-year persistence of the 2014/15 North Pacific marine heatwave. *Nat. Clim. Change* 6:1042–47

Di Lorenzo E, Schneider N, Cobb KM, Franks PJS, Chhak K, et al. 2008. North Pacific Gyre Oscillation links ocean climate and ecosystem change. *Geophys. Res. Lett.* 35:L08607

Ding R, Li J, Tseng Y. 2015. The impact of South Pacific extratropical forcing on ENSO and comparisons with the North Pacific. *Clim. Dyn.* 44:2017–34

Ding R, Li J, Tseng Y, Sun C, Xie F. 2017. Joint impact of North and South Pacific extratropical atmospheric variability on the onset of ENSO events. *J. Geophys. Res. Atmos.* 122:279–98

Ding R, Tseng Y, Di Lorenzo E, Shi L, Yu J-Y, et al. 2022. Multi-year El Niño events tied to the North Pacific Oscillation. *Nat. Commun.* 13:3871

England MH, McGregor S, Spence P, Meehl GA, Timmermann A, et al. 2014. Recent intensification of wind-driven circulation in the Pacific and the ongoing warming hiatus. *Nat. Clim. Change* 4:222–27

Farrell B. 1988. Optimal excitation of neutral Rossby waves. *J. Atmos. Sci.* 45:163–72

Frankignoul C, Gastineau G, Kwon YO. 2017. Estimation of the SST response to anthropogenic and external forcing and its impact on the Atlantic Multidecadal Oscillation and the Pacific Decadal Oscillation. *J. Clim.* 30:9871–95

Frankignoul C, Hasselmann K. 1977. Stochastic climate models, part II: application to sea-surface temperature anomalies and thermocline variability. *Tellus* 29:289–305

Frankignoul C, Reynolds RW. 1983. Testing a dynamical model for mid-latitude sea surface temperature anomalies. *J. Phys. Oceanogr.* 13:1131–45

Frankignoul C, Sennechael N, Kwon YO, Alexander MA. 2011. Influence of the meridional shifts of the Kuroshio and the Oyashio Extensions on the atmospheric circulation. *J. Clim.* 24:762–77

Furtado JC, Di Lorenzo E, Anderson BT, Schneider N. 2012. Linkages between the North Pacific Oscillation and central tropical Pacific SSTs at low frequencies. *Clim. Dyn.* 39:2833–46

Furtado JC, Di Lorenzo E, Schneider N, Bond NA. 2011. North Pacific decadal variability and climate change in the IPCC AR4 models. *J. Clim.* 24:3049–67

Garreaud RD, Battisti DS. 1999. Interannual (ENSO) and interdecadal (ENSO-like) variability in the Southern Hemisphere tropospheric circulation. *J. Clim.* 12:2113–23

Hare SR, Mantua NJ. 2000. Empirical evidence for North Pacific regime shifts in 1977 and 1989. *Prog. Oceanogr.* 47:103–45

Hare SR, Mantua NJ, Francis RC. 1999. Inverse production regimes: Alaska and West Coast Pacific salmon. *Fisheries* 24:6–14

Hasselmann K. 1976. Stochastic climate models part I: theory. *Tellus* 28:473–85
Hoerling MP, Kumar A, Zhong M. 1997. El Niño, La Niña, and the nonlinearity of their teleconnections. *J. Clim.* 10:1769–86
Holbrook NJ, Scannell HA, Sen Gupta A, Benthuysen JA, Feng M, et al. 2019. A global assessment of marine heatwaves and their drivers. *Nat. Commun.* 10:2624
Hoskins BJ, Karoly DJ. 1981. The steady linear response of a spherical atmosphere to thermal and orographic forcing. *J. Atmos. Sci.* 38:1179–96
Hsu HH, Chen YL. 2011. Decadal to bi-decadal rainfall variation in the western Pacific: a footprint of South Pacific decadal variability? *Geophys. Res. Lett.* 38:L03703
Jia F, Cai WJ, Gan BL, Wu LX, Di Lorenzo E. 2021. Enhanced North Pacific impact on El Niño/Southern Oscillation under greenhouse warming. *Nat. Clim. Change* 11:840–47
Joh Y, Di Lorenzo E. 2017. Increasing coupling between NPGO and PDO leads to prolonged marine heatwaves in the northeast Pacific. *Geophys. Res. Lett.* 44:11663–71
Joh Y, Di Lorenzo E. 2019. Interactions between Kuroshio Extension and Central Tropical Pacific lead to preferred decadal-timescale oscillations in Pacific climate. *Sci. Rep.* 9:13558
Joh Y, Di Lorenzo E, Siqueira L, Kirtman BP. 2021. Enhanced interactions of Kuroshio Extension with tropical Pacific in a changing climate. *Sci. Rep.* 11:6247
Knight JR, Folland CK, Scaife AA. 2006. Climate impacts of the Atlantic Multidecadal Oscillation. *Geophys. Res. Lett.* 33:L17706
Knutson TR, Manabe S. 1998. Model assessment of decadal variability and trends in the tropical Pacific Ocean. *J. Clim.* 11:2273–96
Kosaka Y, Xie SP. 2013. Recent global-warming hiatus tied to equatorial Pacific surface cooling. *Nature* 501:403–7
Kucharski F, Ikram F, Molteni F, Farneti R, Kang IS, et al. 2016. Atlantic forcing of Pacific decadal variability. *Clim. Dyn.* 46:2337–51
Kwon YO, Alexander MA, Bond NA, Frankignoul C, Nakamura H, et al. 2010. Role of the Gulf Stream and Kuroshio-Oyashio systems in large-scale atmosphere-ocean interaction: a review. *J. Clim.* 23:3249–81
Larson SM, Kirtman BP. 2014. The Pacific meridional mode as an ENSO precursor and predictor in the North American Multimodel Ensemble. *J. Clim.* 27:7018–32
Larson SM, Pegion KV, Kirtman BP. 2018. The South Pacific meridional mode as a thermally driven source of ENSO amplitude modulation and uncertainty. *J. Clim.* 31:5127–45
Levine AF, McPhaden MJ, Frierson DM. 2017. The impact of the AMO on multidecadal ENSO variability. *Geophys. Res. Lett.* 44:3877–86
Liguori G, Di Lorenzo E. 2018. Meridional modes and increasing Pacific decadal variability under anthropogenic forcing. *Geophys. Res. Lett.* 45:983–91
Liguori G, Di Lorenzo E. 2019. Separating the North and South Pacific Meridional Modes contributions to ENSO and tropical decadal variability. *Geophys. Res. Lett.* 46:906–15
Linkin ME, Nigam S. 2008. The North Pacific Oscillation–west Pacific teleconnection pattern: mature-phase structure and winter impacts. *J. Clim.* 21:1979–97
Liu Z, Alexander M. 2007. Atmospheric bridge, oceanic tunnel, and global climatic teleconnections. *Rev. Geophys.* 45:RG2005
Liu Z, Di Lorenzo E. 2018. Mechanisms and predictability of Pacific decadal variability. *Curr. Clim. Change Rep.* 4:128–44
Lou J, Holbrook NJ, O'Kane TJ. 2019. South Pacific decadal climate variability and potential predictability. *J. Clim.* 32:6051–69
Lou J, O'Kane TJ, Holbrook NJ. 2020. A linear inverse model of tropical and South Pacific seasonal predictability. *J. Clim.* 33:4537–54
Lou J, O'Kane TJ, Holbrook NJ. 2021. A linear inverse model of tropical and South Pacific climate variability: optimal structure and stochastic forcing. *J. Clim.* 34:143–55
Ma X, Chang P, Saravanan R, Montuoro R, Nakamura H, et al. 2017. Importance of resolving Kuroshio front and eddy influence in simulating the North Pacific storm track. *J. Clim.* 30:1861–80
Mantua NJ, Hare SR, Zhang Y, Wallace JM, Francis RC. 1997. A Pacific interdecadal climate oscillation with impacts on salmon production. *Bull. Am. Meteorol. Soc.* 78:1069–79

Martinez-Villalobos C, Vimont DJ. 2017. An analytical framework for understanding tropical meridional modes. *J. Clim.* 30:3303–23
Meehl GA, Arblaster JM, Fasullo JT, Hu AX, Trenberth KE. 2011. Model-based evidence of deep-ocean heat uptake during surface-temperature hiatus periods. *Nat. Clim. Change* 1:360–64
Meehl GA, van Loon H, Arblaster JM. 2017. The role of the Southern Hemisphere semiannual oscillation in the development of a precursor to central and eastern Pacific Southern Oscillation warm events. *Geophys. Res. Lett.* 44:6959–65
Messie M, Chavez F. 2011. Global modes of sea surface temperature variability in relation to regional climate indices. *J. Clim.* 24:4314–31
Min Q, Su J, Zhang R. 2017. Impact of the South and North Pacific meridional modes on the El Niño–Southern Oscillation: observational analysis and comparison. *J. Clim.* 30:1705–20
Monahan AH, Fyfe JC, Ambaum MHP, Stephenson DB, North GR. 2009. Empirical orthogonal functions: The medium is the message. *J. Clim.* 22:6501–14
Na H, Kim KY, Minobe S, Sasaki YN. 2018. Interannual to decadal variability of the upper-ocean heat content in the western North Pacific and its relationship to oceanic and atmospheric variability. *J. Clim.* 31:5107–25
Namias J, Born RM. 1974. Further studies of temporal coherence in North Pacific sea surface temperatures. *J. Geophys. Res.* 79:797–98
Newman M. 2007. Interannual to decadal predictability of tropical and North Pacific sea surface temperatures. *J. Clim.* 20:2333–56
Newman M. 2013. An empirical benchmark for decadal forecasts of global surface temperature anomalies. *J. Clim.* 26:5260–69
Newman M, Alexander MA, Ault TR, Cobb KM, Deser C, et al. 2016. The Pacific Decadal Oscillation, revisited. *J. Clim.* 29:4399–427
Newman M, Alexander MA, Scott JD. 2011. An empirical model of tropical ocean dynamics. *Clim. Dyn.* 37:1823–41
Newman M, Compo GP, Alexander MA. 2003. ENSO-forced variability of the Pacific decadal oscillation. *J. Clim.* 16:3853–57
Newman M, Sardeshmukh PD. 2017. Are we near the predictability limit of tropical Indo-Pacific sea surface temperatures? *Geophys. Res. Lett.* 44:8520–29
Nigam S, Sengupta A, Ruiz-Barradas A. 2020. Atlantic–Pacific links in observed multidecadal SST variability: Is the Atlantic Multidecadal Oscillation's phase reversal orchestrated by the Pacific Decadal Oscillation? *J. Clim.* 33:5479–505
Nurhati IS, Cobb KM, Di Lorenzo E. 2011. Decadal-scale SST and salinity variations in the central tropical Pacific: signatures of natural and anthropogenic climate change. *J. Clim.* 24:3294–308
Okumura YM. 2013. Origins of tropical Pacific decadal variability: role of stochastic atmospheric forcing from the South Pacific. *J. Clim.* 26:9791–96
Penland C, Matrosova L. 1994. A balance condition for stochastic numerical models with application to the El Niño–Southern Oscillation. *J. Clim.* 7:1352–72
Penland C, Matrosova L. 2006. Studies of El Niño and interdecadal variability in tropical sea surface temperatures using a nonnormal filter. *J. Clim.* 19:5796–815
Penland C, Sardeshmukh PD. 1995. The optimal growth of tropical sea surface temperature anomalies. *J. Clim.* 8:1999–2024
Power S, Casey T, Folland C, Colman A, Mehta V. 1999. Inter-decadal modulation of the impact of ENSO on Australia. *Clim. Dyn.* 15:319–24
Power S, Lengaigne M, Capotondi A, Khodri M, Vialard J, et al. 2021. Decadal climate variability in the tropical Pacific: characteristics, causes, predictability, and prospects. *Science* 374:eaay9165
Pozo Buil M, Di Lorenzo E. 2015. Decadal changes in Gulf of Alaska upwelling source waters. *Geophys. Res. Lett.* 42:1488–95
Pozo Buil M, Di Lorenzo E. 2017. Decadal dynamics and predictability of oxygen and subsurface tracers in the California Current System. *Geophys. Res. Lett.* 44:4204–13
Qiu B. 2003. Kuroshio Extension variability and forcing of the Pacific decadal oscillations: responses and potential feedback. *J. Phys. Oceanogr.* 33:2465–82

Qiu B, Chen S. 2005. Variability of the Kuroshio Extension jet, recirculation gyre, and mesoscale eddies on decadal time scales. *J. Phys. Oceanogr.* 35:2090–103
Qiu B, Chen S, Schneider N, Taguchi B. 2014. A coupled decadal prediction of the dynamic state of the Kuroshio Extension system. *J. Clim.* 27:1751–64
Qiu B, Schneider N, Chen S. 2007. Coupled decadal variability in the North Pacific: an observationally constrained idealized model. *J. Clim.* 20:3602–20
Rayner NA, Parker DE, Horton EB, Folland CK, Alexander LV, et al. 2003. Global analyses of sea surface temperature, sea ice, and night marine air temperature since the late nineteenth century. *J. Geophys. Res. Atmos.* 108:4407
Rogers JC. 1981. The North Pacific Oscillation. *J. Climatol.* 1:39–57
Rudnick DL, Davis RE. 2003. Red noise and regime shifts. *Deep-Sea Res. I* 50:691–99
Sardeshmukh PD, Hoskins BJ. 1988. The generation of global rotational flow by steady idealized tropical divergence. *J. Atmos. Sci.* 45:1228–51
Sasaki YN, Schneider N. 2011. Decadal shifts of the Kuroshio Extension jet: application of thin-jet theory. *J. Phys. Oceanogr.* 41:979–93
Schneider N, Cornuelle BD. 2005. The forcing of the Pacific decadal oscillation. *J. Clim.* 18:4355–73
Schneider N, Miller AJ. 2001. Predicting western North Pacific Ocean climate. *J. Clim.* 14:3997–4002
Schneider N, Miller AJ, Alexander MA, Deser C. 1999. Subduction of decadal North Pacific temperature anomalies: observations and dynamics. *J. Phys. Oceanogr.* 29:1056–70
Schwing FB, Murphree T, deWitt L, Green PM. 2002. The evolution of oceanic and atmospheric anomalies in the northeast Pacific during the El Niño and La Niña events of 1995–2001. *Prog. Oceanogr.* 54:459–91
Screen JA, Francis JA. 2016. Contribution of sea-ice loss to Arctic amplification is regulated by Pacific Ocean decadal variability. *Nat. Clim. Change* 6:856–60
Seager R, Henderson N. 2016. On the role of tropical ocean forcing of the persistent North American West Coast ridge of winter 2013/14. *J. Clim.* 29:8027–49
Shakun JD, Shaman J. 2009. Tropical origins of North and South Pacific decadal variability. *Geophys. Res. Lett.* 36:L19711
Siqueira L, Kirtman BP, Laurindo LC. 2021. Forecasting remote atmospheric responses to decadal Kuroshio stability transitions. *J. Clim.* 34:379–95
Smirnov D, Newman M, Alexander MA, Kwon Y-O, Frankignoul C. 2015. Investigating the local atmospheric response to a realistic shift in the Oyashio sea surface temperature front. *J. Clim.* 28:1126–47
Smith TM, Reynolds RW, Peterson TC, Lawrimore J. 2008. Improvements to NOAA's historical merged land-ocean surface temperature analysis (1880–2006). *J. Clim.* 21:2283–96
Stuecker MF. 2018. Revisiting the Pacific Meridional Mode. *Sci. Rep.* 8:3216
Swain DL. 2015. A tale of two California droughts: lessons amidst record warmth and dryness in a region of complex physical and human geography. *Geophys. Res. Lett.* 42:9999–10003
Taguchi B, Schneider N. 2014. Origin of decadal-scale, eastward-propagating heat content anomalies in the North Pacific. *J. Clim.* 27:7568–86
Taguchi B, Xie SP, Schneider N, Nonaka M, Sasaki H, Sasai Y. 2007. Decadal variability of the Kuroshio Extension: observations and an eddy-resolving model hindcast. *J. Clim.* 20:2357–77
Taschetto AS, Ummenhofer CC, Stuecker MF, Dommenget D, Ashok K, et al. 2020. ENSO atmospheric teleconnections. In *El Niño Southern Oscillation in a Changing Climate*, ed. MJ McPhaden, A Santoso, W Cai, pp. 309–35. Washington, DC: Am. Geophys. Union
Trenberth KE, Hurrell JW. 1994. Decadal atmosphere-ocean variations in the Pacific. *Clim. Dyn.* 9:303–19
van der Sleen P, Zuidema PA, Morrongiello J, Ong JLJ, Rykaczewski R, et al. 2022. Interannual temperature variability is a principal driver of low-frequency fluctuations in marine fish populations. *Commun. Biol.* 5:28
Vimont DJ. 2005. The contribution of the interannual ENSO cycle to the spatial pattern of decadal ENSO-like variability. *J. Clim.* 18:2080–92
Vimont DJ. 2010. Transient growth of thermodynamically coupled variations in the tropics under an equatorially symmetric mean. *J. Clim.* 23:5771–89
Vimont DJ, Alexander MA, Fontaine A. 2009. Midlatitude excitation of tropical variability in the Pacific: the role of thermodynamic coupling and seasonality. *J. Clim.* 22:518–34

Vimont DJ, Alexander MA, Newman M. 2014. Optimal growth of Central and East Pacific ENSO events. *Geophys. Res. Lett.* 41:4027–34
Vimont DJ, Battisti DS, Hirst AC. 2001. Footprinting: a seasonal connection between the tropics and mid-latitudes. *Geophys. Res. Lett.* 28:3923–26
Vimont DJ, Wallace JM, Battisti DS. 2003. The seasonal footprinting mechanism in the Pacific: implications for ENSO. *J. Clim.* 16:2668–75
Wang C. 2018. A review of ENSO theories. *Natl. Sci. Rev.* 5:813–25
Wang C, Deser C, Yu J-Y, DiNezio P, Clement A. 2017. El Niño and Southern Oscillation (ENSO): a review. In *Coral Reefs of the Eastern Tropical Pacific*, ed. P Glymn, D Manzello, I Enochs, pp. 85–106. Dordrecht, Neth.: Springer
Watanabe M, Kamae Y, Yoshimori M, Oka A, Sato M, et al. 2013. Strengthening of ocean heat uptake efficiency associated with the recent climate hiatus. *Geophys. Res. Lett.* 40:3175–79
Wei W, Yan Z, Li Z. 2021. Influence of Pacific Decadal Oscillation on global precipitation extremes. *Environ. Res. Lett.* 16:044031
Xie S-P. 1999. A dynamic ocean–atmosphere model of the tropical Atlantic decadal variability. *J. Clim.* 12:64–70
Xu T, Newman M, Capotondi A, Di Lorenzo E. 2021. The continuum of northeast Pacific marine heatwaves and their relationship to the tropical Pacific. *Geophys. Res. Lett.* 48:2020GL090661
Yang X-Y, Wang G, Keenlyside N. 2020. The Arctic sea ice extent change connected to Pacific decadal variability. *Cryosphere* 14:693–708
Yang Y-M, An S-I, Wang B, Park JH. 2020. A global-scale multidecadal variability driven by Atlantic multidecadal oscillation. *Natl. Sci. Rev.* 7:1190–97
Yati E, Minobe S, Mantua N, Ito S, Di Lorenzo E. 2020. Marine ecosystem variations over the North Pacific and their linkage to large-scale climate variability and change. *Front. Mar. Sci.* 7:578165
You Y, Furtado JC. 2017. The role of South Pacific atmospheric variability in the development of different types of ENSO. *Geophys. Res. Lett.* 44:7438–46
You Y, Furtado JC. 2018. The South Pacific meridional mode and its role in tropical Pacific climate variability. *J. Clim.* 31:10141–63
Zhang H, Clement A, Di Nezio P. 2014. The South Pacific meridional mode: a mechanism for ENSO-like variability. *J. Clim.* 27:769–83
Zhang Y, Wallace JM, Battisti DS. 1997. ENSO-like interdecadal variability: 1900–93. *J. Clim.* 10:1004–20
Zhang Y, Xie S-P, Kosaka Y, Yang J-C. 2018. Pacific Decadal Oscillation: tropical Pacific forcing versus internal variability. *J. Clim.* 31:8265–79
Zhao Y, Di Lorenzo E. 2020. The impacts of extra-tropical ENSO precursors on tropical Pacific decadal-scale variability. *Sci. Rep.* 10:3031
Zhao Y, Di Lorenzo E, Sun D, Stevenson S. 2021a. Tropical Pacific decadal variability and ENSO precursor in CMIP5 models. *J. Clim.* 34:1023–45
Zhao Y, Newman M, Capotondi A, Di Lorenzo E, Sun D. 2021b. Removing the effects of tropical dynamics from North Pacific climate variability. *J. Clim.* 34:9249–65
Zheng J, Wang F. 2017. On the formation of the South Pacific quadrupole mode. *Theor. Appl. Climatol.* 130:331–44

Annual Review of Marine Science

Volume 15, 2023

Contents

Errata

An online log of corrections to *Annual Review of Marine Science* articles may be found at http://www.annualreviews.org/errata/marine